COMPUTATIONAL FLUID DYNAMICS (CFD) MODELING OF A PILOT-SCALE MEMBRANE FILTRATION TECHNOLOGY TO TREAT OILY WASTEWATER

By

Mahsa Keyvan Hosseini

Submitted in partial fulfillment of the requirements
for the degree of Master of Applied Science

at

Dalhousie University
Halifax, Nova Scotia
November 2022

To my Family for their unconditional love, support, and encouragement

Table of Contents

List of Tables

List of Figures

Abstract

In this study, a pilot-scale membrane filtration system for the treatment of oily wastewater through a comprehensive three-dimensional (3D) computational fluid dynamics (CFD) modeling was investigated. The model was designed and developed based on the characteristics of the pilot-scale system and validated using oil removal efficiency and average transmembrane pressure (TMP) obtained by the experimental data for two types of oily wastewater containing heavy crude oil, Cold Lake Dilbit (CLD) and light crude oil, Very Low Sulfur Fuel Oil (VLSFO). Results showed that the system met the International Convention for the Prevention of Pollution from Ships (MARPOL) 73/78 regulation when the inlet oil concentration was at the threshold of 270 mg/L and 330 mg/L containing CLD and VLSFO, respectively. In addition, the model was used to scale up for field-scale applications at a capacity of 10,000 L/h and results demonstrated that the oil removal efficiency was above 91%.

List of Abbreviations and Symbols Used

API	American Petroleum Institute
BTEX	Benzene, Toluene, Ethylbenzene and Xylene
CFD	Computational Fluid Dynamics
CFR	Crossflow Rate
CFV	Crossflow Velocity
CLD	Cold Lake Dilbit
COD	Chemical Oxygen Demand
FDM	Finite Difference Method
FEM	Finite Element Method
FVM	Finite Volume Method
HF	Hollow Fiber
ISCO	International Spill Control Organization
MBR	Membrane Bioreactor
MF	Microfiltration
NF	Nanofiltration
PAHs	Polycyclic Aromatic Hydrocarbons
PAN	Polyacrylonitrile
PDE	Partial Differential Equation
PES	Polyether Sulfone
PLC	Programable Logic Controller

ppm	Parts per Million
PS	Polysulfone
PTFE	Polytetrafluoroethylene
PVC	Polyvinylchloride
PVDF	Polyvinylidenedifluoride
RE	Relative Error
RO	Reverse Osmosis
TDS	Total Dissolved Solids
TMP	Transmembrane Pressure
TOC	Total Organic Carbon
TSS	Total Suspended Solids
UF	Ultrafiltration
VLSFO	Very Low Sulfur Fuel Oil
VOC	Volatile Organic Compound

grad	Gradient
ρ	Fluid Density
μ	Fluid Dynamic Viscosity
u	Fluid Velocity
d	Inside Diameter of the Pipe
Re	Reynolds Number

D_{AB}	Diffusion Coefficient of Component A in Solution B
J_A	Flux of Component A
$\frac{\partial c_A}{\partial z}$	Concentration Gradient of Component A
P_{in}	Pressure at the Inlet of the Inner Casing
P_{out}	Pressure at the Outlet of the Inner Casing
P_{perm}	Pressure at the Outlet of the Outer Casing
Q_v	Volumetric Flow Rate
A	Cross-Sectional Area
J	Membrane Flux
κ	Membrane Intrinsic Permeability
δ_m	Membrane Thickness
R_m	Membrane Hydraulic Resistance
t	Time
f	Body Force
p	Pressure
$ø$	Volume Fraction of Each Phase (Gas/liquid)
Indice l	Refers to Liquid
Indice g	Refers to Gas
m_{gl}	Mass Transfer Rate from Gas to Liquid
E_0	Eotvos Number

σ	Surface Tension Coefficient
d_b	Bubble Diameter
U_{slip}	Slip Velocity
f_d	Drag Force
C_d	Drag Coefficient
g	Gravity Acceleration
$N_{\rho_g \emptyset_g}$	Gas Mass Flux
n	Vector Normal to the Boundary
K	A Term Related to Viscous Force
ε_p	Membrane Porosity
C_i	Oil Concentration in the Membrane Tank
D_i	Diffusion Coefficient of Oil in Water
R_i	Adsorption and Desorption Rate
$D_{D,i}$	Dispersion Tensor
$D_{e,i}$	Effective Diffusivity
S_i	Source Term
$Q_{field\_throughput}$	Field Throughput
$Q_{max\_throughput\ (current\_system)}$	Maximum Throughput in the Current System
N_{unit}	Total Number of Units
N_{unit_x}	Number of Units in the x Direction
N_{unit_y}	Number of Units in the y Direction

$N_{aerator\_x}$	Number of Aerators in the x Direction
$N_{aerator\_y}$	Number of Aerators in the y Direction
$N_{aerator}$	Total Number of Aerators
Mem_{width}	Membrane Width
Mem_{depth}	Membrane Depth
Mem_{height}	Membrane Height
S_w	Side Gap in the x Direction
S_d	Side Gap in the y Direction
$Tank_{length}$	Length of the Membrane Tank
$Tank_{width}$	Width of the Membrane Tank
$Q_{aeration\_upscaled}$	Aeration Flow Rate in Upscaled System
$E_{oil,removal\_Exp}$	Oil Removal Efficiency (Experiment)
$E_{oil,removal\_Model}$	Oil Removal Efficiency (Model)
TMP_{Exp}	Transmembrane Pressure (Experiment)
TMP_{Model}	Transmembrane Pressure (Model)
τ	Shear Stress
$\frac{du_x}{dy}$	Shear Rate
μm	Micrometer
nm	Nanometer
$2D$	Two-Dimensional
$3D$	Three-Dimensional
C_{oil_inside}	Oil Concentration Inside the Membrane

$C_{oil\_outside}$	Oil Concentration Outside the Membrane

Acknowledgements

I would like to express my sincere gratitude to my supervisor Professor Lei Liu for his trust and support. His point of view on scientific subjects is exemplary that has made me think critically and be creative. His contributions of time, patience, energy, and dedication to my success are profoundly appreciated.

I am grateful to be informed of the valuable and technical comments of my committee members Professor Margaret Walsh and Professor Haibo Niu.

I gratefully acknowledge the financial support provided to this project by Department of Fisheries and Oceans Canada (DFO), Canada Coast Guard (CCG), Multi-Partner Research Initiative (MPRI) program, the National Science and Engineering Research Council (NSERC), and the Faculty of Graduate Studies for the FGS scholarship. I would like to express my special gratitude to Dr. Kenneth Lee for MPRI program and providing a scientific and friendly atmosphere for students to learn.

I am thankful to Dr. Hesam Hafezi during the first year of this journey to guide and help me. I appreciate Dr. Naznin Sultana Daisy for her guidance, as well.

During experimental runs in the laboratory and modeling process, I cannot overlook the support of my twin sister Parisa without whom this work cannot be fulfilled. We came across disappointing and encouraging moments together and tried to learn how to be stronger against challenges and I deeply appreciate her to accompany me in this journey. Also, I appreciate the MPRI team members for their kind and helpful comments and guidance during this project. In addition, Jesse Keane in the mining laboratory, Heather

Daurie in water laboratory, Daniel Chevalier, and Gerald Fraser in the chemical engineering laboratory helped a lot and I am thankful. I really appreciate Professor Navid Bahrani and his students for their kind help. I also thank my fellow graduate friends for their help and kindness.

Last but not least, I am extremely thankful to my father for his support, advice, and encouragement in all walks of life and to my mother who has injected me positive energy. You two have been the fountain of inspiration for me to pursue what truly means in life. I am also grateful to my nice brother, Parsa.

CHAPTER 1 INTRODUCTION

This chapter includes the background defining the problem statement and rationale of this study, and outlines the research objectives, the approach used, and the thesis layout.

1.1. Background

Oily wastewater is generated from various sources such as petroleum industry, leather processing, metal processing, and shipping and transport (Sanghamitra et al., 2021). The discharge of this type of wastewater into the environment negatively affects ecosystem and human health due to the existence of toxic compounds, such as volatile organic compounds (VOCs), polycyclic aromatic hydrocarbons (PAHs), phenols, and heavy metals (Han et al., 2019; Abuhasel et al., 2021; Sanghamitra et al., 2021). A portion of discharged oily wastewater to the aquatic environment is related to marine oil spill incidents. To reduce the negative environmental impacts of this type of oily wastewater, the vessel-based operation has been used throughout marine oil spill response operations (Herndon, 2005; Han et al., 2019). This method of operation leads to the collection of a large volume of water together with the spilled oil. Oil and water mixture is stored in a temporary storage container on ships/barges and when the mixture has settled for a certain time, the oil is naturally separated and remained at the top layer of the water through the gravity separation process (Han et al., 2019). Following this separation, the decanted water still has a large quantity of dispersed, emulsified, and dissolved hydrocarbons that are potential pollutants to the oceans and marine creatures if discharged without adequate and efficient treatment.

Disposing decanted water at sea is typically regulated by an acceptable overall oil content, under the International Convention for the Prevention of Pollution from Ships (MARPOL 73/78). This regulation was suggested by the International Spill Control Organization (ISCO) which states that oil content of the discharge cannot surpass 15 ppm; however, no oil content is allowed in Special Areas such as the Antarctic or the Great Lakes (Herndon, 2005; ISCO, 2022). In some cases, even when the total oil content meets the regulations, decanted water still contains persistent, bio-accumulative, carcinogenic, and mutagenic pollutants such as PAHs and phenols (Rashid et al., 2022) which pose barriers to permit discharge of decanted water at sea. Therefore, in Canada, the disposal of decanted water back into the ocean is banned by Canada Fisheries Act (Government of Canada, 2018), and decanted water must be barged to shore for discharge (Herndon, 2005). This drastically restricts the capacity of response and efficacy of oil spill response operation as a result of limited temporary storage space in barges and long time and high cost of transportation (Liu et al., 2022). Finding effective and efficient onsite treatment technologies to allow wastewater discharge is one of the most important measures to improve the capabilities of the oil spill response operation and protect the ocean.

Membrane filtration technology provides advantages such as high removal efficiency and low secondary pollution. More importantly, this technology is able to treat oily wastewater containing a small oil droplet size below 20 μm which is difficult to remove by conventional methods (Zhang et al., 2020; Varjani et al., 2020). In addition, this technique does not require biological processes and only includes physical separation which is simple to operate. Unlike biological-based technology, membrane process is not impacted by environmental factors such as a change in feed composition and level of oxygen (Meena

et al., 2019). It does not generate CO_2 and large quantity of greenhouse gas (Lateef et al., 2013). However, the main challenge in the membrane filtration system is membrane fouling which refers to the accumulation of substances on the membrane surface and within the pores. This increases transmembrane pressure (TMP), decreases permeate production and membrane lifespan (Bagheri & Mirbagheri, 2018).

Reviewing previous research projects demonstrates that most of the numerical studies conducted to date has evaluated the membrane performance to treat different types of wastewater at bench-scale membrane filtration systems under the constant TMP using a two-dimensional (2D) computational fluid dynamics (CFD) model (Keir & Jegatheesan, 2014; Behroozi et al., 2019). For example, Vinther et al. (2014) simulated and investigated the treatment process of wastewater containing dextran using a 2D CFD model in a bench-scale membrane filtration system; Nowee et al. (2017) developed a 2D mathematical model for phenol removal in a bench-scale membrane bioreactor (MBR); Maarefian et al. (2017) modeled a bench-scale MBR system to remove chemical oxygen demand (COD) from high saline refinery wastewater under the constant TMP. However, very limited numerical studies investigated oil removal efficiency in a membrane filtration system operating under the constant flux in a pilot and/or large scale using a three-dimensional (3D) CFD model (Pawloski, 2016; Ismail et al., 2020; Naim et al., 2021). Operating pilot- and/or large-scale systems in a real-world condition has challenges and difficulties such as controlling experimental conditions (e.g., adjusting flux, TMP, and aeration flow rate) and high cost (e.g., in terms of construction and fabrication of the system, purchase of the membranes, pumps, and air blowers) (Pawloski, 2016). Therefore, accessibility to the pilot- and/or large-scale systems in laboratories, and consequently, their experimental data for model

validation has been limited for most researchers. In addition, operating a membrane filtration system under the constant TMP specifically at large scales leads to a serious membrane fouling (Hussain, 2019). This is due to the fact that solute particles move towards the membrane surface more rapidly than they are transported away, leading to more particles being accumulated on the membrane surface at the constant TMP compared to the constant flux. Therefore, simulating and operating a membrane filtration system under the constant flux would be more beneficial for industrial applications due to a stable permeate production rate with insignificant membrane fouling and the ease of membrane cleaning (Hussain, 2019; Keyvan Hosseini et al., 2023).

The majority of the previous numerical research investigated the impacts of turbulency promoter techniques such as baffles, spacers, and gas sparging on the bench-scale membrane filtration process (Santos et al., 2007; Wardeh & Morvan, 2008; Liu et al., 2009). For example, Khalili-Garakani et al. (2011) and Yan et al. (2016) investigated the hydrodynamic behavior and the impact of aeration flow rate on shear stress in a bench-scale MBR. However, these studies did not consider the impact of aeration on membrane fouling and did not assess the hydrodynamic behavior of a pilot-scale membrane filtration system containing different types of oily wastewater (i.e., heavy and light crude oils).

To address the knowledge gaps, in this research project, CFD modeling was used to investigate oily wastewater treatment in a pilot scale membrane filtration system under the constant flux using a 3D CFD model. CFD is a successful approach that can help investigate treatment processes and hydrodynamic behavior in any geometrical configurations and module scales (Samstag et al., 2016; Guo et al., 2017; Shi et al., 2021;

Poormohamadian et al., 2022). In this method, the geometry is decomposed into finite volumes and transport equations such as mass, momentum, species, and energy balance are discretized for the whole of the finite volumes/computational mesh, and then, solved numerically (Lukitsch et al., 2020).

1.2. Objectives

The overall objective of this study was to investigate the pilot-scale membrane filtration system for the treatment of oily wastewater through a comprehensive 3D CFD modeling and used the model to scale up the system and explored its capability in a larger-scale field application. The specific research objectives were as follows.

- Construct and develop a 3D CFD model for a pilot-scale membrane filtration system treating oily wastewater under the constant flux
- Investigate the hydrodynamic behavior of the pilot-scale unit and the impact of different operating parameters on oil removal efficiency and TMP
- Scale up a pilot-scale system for larger-scale field applications and explore its potential as an onsite treatment technology for oil spill response operations

In order to fulfill the research objectives, the model geometry was designed based on the dimensions of the pilot-scale membrane filtration system. The model was then constructed with free tetrahedral geometry mesh configuration, and mesh independence analysis was conducted to estimate the optimum simulation grid size for the simulation domain. In the modeling process, different physics such as fluid flow, Darcy's law, and mass transfer were integrated with considering the characteristics of oily wastewater and membranes. The

model was validated according to the oil removal efficiency and average TMP obtained by the experimental results. The validated model was then used to investigate the hydrodynamic behavior of the system at an unsteady-state condition of fluid flow module with measuring gas volume fraction, gas and liquid velocity in the membrane tank, and shear stress on the membrane surface. Then, a fluid flow module at a steady-state condition and Darcy's law and mass transfer modules at an unsteady-state condition were coupled and solved to investigate the impact of operating parameters on system oil removal efficiency. Following that, the model was used to scale up through suggesting an upscaling index. This modeling framework can provide a comprehensive investigation regarding the hydrodynamic condition inside the pilot-scale membrane filtration system which has been challenging to determine in a real-world application. Furthermore, it can predict the capability of the system to treat oily wastewater for both pilot-scale and larger-scale field applications and save cost and energy for oil spill response team due to reducing the number of experimental runs.

1.3. Thesis Outline

This thesis is split into five chapters. Chapter 1 determines the problem statement and motivations of this research, and outlines the research objectives, approach, significance, and thesis organization. Chapter 2 contains the fundamentals of membrane filtration technology and CFD followed by a literature review of previous works related to CFD simulation to model membrane processes and scale-up. A review of the literature has yielded information on the background of simulating free flow and membrane filtration technology through CFD. An explanation of the membrane-based simulation and the

effectiveness of the method is included in four subsections. Knowledge gaps have been identified at the end of the chapter. Chapter 3 provides a detailed methodology of the techniques applied to fulfill the research goals. The research plan was divided into five primary phases; the steps included designing and constructing a 3D CFD model for a pilot-scale membrane filtration system, validating the model based on experimental data, investigating system hydrodynamics, conducting parametric study analysis, and using the model for upscaling design in the field-scale applications. The results achieved through various methods, as well as the analysis and discussion of the findings, are addressed in Chapter 4. Chapter 5 summarizes the main findings and identifies areas that may require additional research. Finally, references used for this study have been mentioned in the last section.

CHAPTER 2 LITERATURE REVIEW

2.1. Oily Wastewater and Treatment Techniques

Oily wastewater is a mixture of dissolved and particulate solids, organic and inorganic matters, salts, and hazardous chemicals; major parameters in this type of wastewater include chemical oxygen demand (COD), total suspended solid (TSS), total organic carbon (TOC), and total dissolved solid (TDS) with the quantities of 1,220 to 2,600 mg/L, 1.2 to 1,000 mg/L, 0 to 1,500 mg/L, and 100 to 400,000 mg/L, respectively. It also contains benzene, toluene, ethylbenzene, and xylene (BTEX) with the amounts of 0.032 to 778.51 mg/L, 0.58 to 5.86 mg/L, 0.026 to 399.84 mg/L, and 0.01 to 1.29 mg/L, respectively (Al-Ghouti et al., 2019; Ullah et al., 2021). Depending on the size and stability of the oil droplets, oil in wastewater has four physical forms; free-floating oil contains large droplets (≥150 μm) and is easily removed by conventional gravitational separation approaches, dispersed oil has droplet sizes ranging from 20 to 150 μm and is quite simple to be removed by gravitational processes and/or stabilizing agents. Emulsified oil with an oil droplet size of less than 20 μm and dissolved oil with an oil droplet size of less than 5 μm are extremely difficult to be removed and require other types of techniques (Munirasu et al., 2016; Varjani et al., 2020; Kallem et al., 2021; Medeiros et al., 2022). Membrane filtration technology has been effective to remove small oil droplets (below 20 μm) with low space requirement, low chemical usage, and low waste generation (Kujawa et al., 2017; Obotey Ezugbe & Rathilal, 2020). Hence, it is desired over other techniques achieving selective, effective, and consistent separation of pollutants (Abuhasel et al., 2021).

2.2. Membrane Filtration Technology

Membrane technology is a state-of-the-art separation method that demonstrates continued promise for technical growth and wide-scale commercialization. This technology is progressively finding its way into the growing engineering fields of the oily wastewater treatment industry (Theodore & Ricci, 2010a). In this section, fundamentals of membrane technology such as major mechanisms and effective factors in membrane filtration, membrane fouling, different types of membranes, membrane configuration, and its operation mode have been discussed.

2.2.1. Major Mechanisms of Membrane Filtration Technology

A membrane is a barrier separating two phases from each other by restricting the movement of components in a selective style (Judd, 2010; Obotey Ezugbe & Rathilal, 2020). During the membrane filtration process, different types of driving forces can be imposed (i.e., pressure-driven, osmotic-driven, and thermally-driven), and convection and diffusion are the most significant transport mechanisms in membrane processes for wastewater treatment (Gkotsis et al., 2014; Le & Nunes, 2016). The bulk fluid rather than any dissolved or suspended components causes convection; therefore, convective transport occurs when a liquid flows (Stephenson et al., 2000). In a flowing liquid, flow rate determines the nature of the flow regime. The flow is described as turbulent at high flow rates and as laminar at low flow rates (Stephenson et al., 2000). The Reynolds number (Re) (Eq. (2.1)) is a dimensionless number indicating the condition of the fluid flow in terms of being laminar and turbulent. In the laminar flow regime, fluid moves slowly and no eddies and macroscopic mixing of various segments of the fluid is seen. In contrast, a turbulent

flow regime is described by eddies and macroscopic currents when the Re is more than 2,100 in a pipe (Bird et al., 2002; Theodore & Ricci, 2010b). This dimensionless number depends on the fluid velocity, density, viscosity, and the length characteristic of the system; as an example, the characteristic length for pipes is the inside diameter.

$$\mathrm{Re} = \frac{\rho u d}{\mu} \tag{2.1}$$

where d is the inside diameter of the pipe (m), u is the fluid velocity (m/s), ρ is fluid density (kg/m^3), and μ is the fluid dynamic viscosity (Pa·s).

Brownian diffusion results from the transport of individual ions, atoms, or molecules from an area of high concentration to an area of low concentration (Stephenson et al., 2000). The diffusion coefficient (D_{AB}) of component A in solution B is a measure of its diffusive mobility and is specified as the ratio of its flux, J_A, to its concentration gradient as shown in Eq. (2.2).

$$J_A = -D_{AB} \frac{\partial c_A}{\partial z} \tag{2.2}$$

The concentration gradient term shows the changes of the concentration, C_A in the z direction. The negative sign shows diffusion from high-level to low-level concentrations (Theodore & Ricci, 2010b).

2.2.2. Effective Factors in Membrane Filtration Technology

In membrane processes treating oily wastewater, the most important operating parameters are TMP, flux, crossflow velocity (CFV), and inlet oil concentration (Behroozi & Ataabadi, 2021). These parameters can affect the efficiency of the membrane performance

and membrane fouling. TMP is mostly defined as the difference between average feed pressure and the permeate pressure which is shown in Eq. (2.3).

$$TMP = \frac{(p_{in} + p_{out})}{2} - p_{perm} \tag{2.3}$$

where P_{in} is the pressure at the inlet, P_{out} is the pressure at the outlet of the inner casing, and P_{perm} is pressure at the outlet of the outer casing (Vinther et al., 2014).

Membrane flux is defined as the permeate flow per unit area of the membrane and depends on hydraulic resistance, cake layer thickness, and driving force (Izadi et al., 2018). In addition, flux shows the rate of TMP increase with time, indicating how often the membrane requires to be cleaned and the methods adopted for cleaning (Judd, 2016).

CFV is the linear velocity of the flow tangential to the surface of the membrane and calculated based on Eq. (2.4).

$$CFV = \frac{Q_V}{A} \tag{2.4}$$

where CFV is crossflow velocity (m/s), Q_v is the volumetric flow rate in a flow channel (L/min), and A is the cross-sectional area of the flow channel (m^2) (Sterlitech, 2022). Enhancing CFV in a system causes high membrane flux and low membrane fouling due to increase in turbulency and Re inside the system which results in increasing shear stress and decreasing the accumulation of substances on the surface of the membrane (Behroozi & Ataabadi, 2021). However, when CFV goes beyond a certain threshold, it increases TMP and membrane fouling as a result of reduction of larger particles deposition; therefore, cake layer is mainly formed by small particles which are denser and results in increasing TMP

and membrane fouling (Du et al., 2020). Inlet oil concentration increases the accumulation of oil on the surface of the membrane because of increasing collision of oil droplets and forming larger oil droplets (Behroozi & Ataabadi, 2021).

2.2.3. Membrane Fouling

Membrane fouling is defined as the deposition of particles either on the membrane surface or within the membrane pores. The fouling layer blocks the pores of the membrane and decreases the membrane performance efficiency (Zoubeik, 2018). Membrane fouling happens as a result of five mechanisms including adsorption to membrane walls and pores, membrane pore blocking, concentration polarization, cake layer formation on the surface of the membrane, and cake layer compression (Zoubeik, 2018). The mechanism of membrane fouling is also explained by filtration resistance which is included in Darcy's law (Eq. (2.5)). This law describes that permeate flow is proportional to the pressure applied and the membrane permeability. The resistance is inversely related to the permeability of the membrane (Eq. (2.6)) (Habibi, 2014).

$$J = \frac{\kappa TMP}{\mu \delta_m} = \frac{TMP}{\mu R_m} \tag{2.5}$$

$$R_m = \frac{\delta_m}{\kappa} \tag{2.6}$$

where J is the permeate flow per unit surface of the membrane (m/s), TMP is transmembrane pressure (Pa), μ is the fluid viscosity (Pa·s), κ is the membrane intrinsic permeability (m^2), δ_m is the membrane thickness (m), and R_m is the membrane hydraulic resistance (m^{-1}) (Habibi, 2014).

During oily wastewater treatment, when oil covers the membrane pores, the membrane active layer becomes hydrophobic and this decreases the membrane permeability toward water (Madaeni et al., 2013). Membrane is fouled by oil due to different reasons such as oil droplets accumulation on the surface of the membrane (i.e., forming cake layer and/or concentration polarization), penetrating oil droplets into membrane pores and adsorption on the membrane surface. This phenomenon is due to the permeation drag leading to decrease volume porosity, increase fouling resistance, and reduce flux (Hesampour et al., 2008). Concentration polarization is a common issue which refers to the accumulation of oil droplets at the membrane surface, and therefore, oil concentration on the membrane surface becomes higher than the bulk fluid. In this condition due to the concentration gradient towards the bulk fluid, back diffusion happens. Oily wastewater is entering the membrane filtration system as homogeneous emulsion. A nonzero velocity component towards the membrane leads droplets of oil to be migrated towards the membrane surface and be collected on top of the surface generating concentration gradient (Zoubeik, 2018). Effective parameters such as TMP, flux, and CFV should be optimized to balance flux reduction, mitigate membrane fouling, and prolong the membrane lifespan (Zoubeik, 2018).

2.2.4. Membrane Type

Membranes are classified into two types based on the materials used to construct such as polymeric and ceramic. Ceramic or inorganic membranes consist of materials such as silica, metal oxides, or carbon; they offer excellent chemical stability and long lifespan, and their usage in industrial oil recovery applications is a modern technology. Although

these membranes are susceptible to fouling, rigorous cleaning procedures can restore the flux decline. The main drawbacks of ceramic membrane are high production costs and weight (Deriszadeh et al., 2010; Emani et al., 2014; Dickhout et al., 2017).

Polymeric membranes are used in various industrial separation processes; polymers such as cellulose derivatives, polyvinylidenedifluoride (PVDF), polysulfone (PS), polyether sulfone (PES), polyacrylonitrile (PAN), polytetrafluoroethylene (PTFE), and polyvinylchloride (PVC) have been used to construct polymeric membranes (Lalia et al., 2013). These membranes can be adjusted to the exact requirements of the process in which they are utilized, allowing for selective separation. Selecting a polymeric membrane for a certain purpose is important because the polymer must have the proper affinity and be able to tolerate the treatment condition (Lalia et al., 2013). Although PVDF, PS, and PAN membranes have been extensively used in oily wastewater treatment (Baig et al., 2022), they have some disadvantages. PVDF membranes are fouled rapidly which is a major challenge in their industrial applications (Otitoju et al., 2016). The PS membranes have shown weak mechanical stability, low binding forces, and bulky structure between fibers (Abdelrasoul et al., 2015). PAN membranes have low porosity, low permeance, and weak antifouling performance (Baig et al., 2022). However, PTFE membranes have high chemical resistance, high thermal stability, and mechanical strength (Li et al., 2018); therefore, it can be a suitable membrane material for harsh treatment conditions such as oily wastewater.

In addition, membrane has been categorized based on the difference between the pressure-driven membrane processes including microfiltration (MF), ultrafiltration (UF),

nanofiltration (NF), and reverse osmosis (RO) (Sidney & Srinivasa, 1964). MF has the biggest pore size and is capable of filtering suspended particles and microorganisms ranging from 0.1 to 5 μm. Macromolecules and soluble solids (inorganic salts) pass through MF membrane, but this membrane can intercept suspended solids, bacteria, and macromolecular colloids. The operating pressure of MF is generally between 0.01 and 0.2 MPa (Rezakazemi et al., 2018; Yang, 2020). The pore size of UF is smaller than that of MF and they can be used to separate aromas, viruses, colors, and colloidal organic substances in the range of 0.001 to 0.1 μm. The operating pressure of UF is generally between 0.05 and 0.6 MPa (Hu et al., 2010; Igunnu & Chen, 2014; Yang, 2020). In both MF and UF membranes, the removal mechanism is sieving and transport mechanism is convection (Cao, 2016). Another type of membrane separation technique used in water purification is NF; this membrane can remove particles ranging between 0.0001 to 0.01 μm (Pabby et al., 2015). The operating pressure of NF is generally between 0.5 and 1.5 MPa (Yang, 2020). RO has the highest separation accuracy, which can successfully intercept all dissolved salts and organics in the range of 0.0001 to 0.001 μm (Malaeb & Ayoub, 2011). It is mainly utilized for salt removal of industrial water, desalination of brackish water and seawater, and wastewater treatment. The operating pressure of RO is generally between 1 and 10 MPa (Yang, 2020). Removal mechanism and transport mechanism in NF and RO membranes are diffusion (Cao, 2016).

2.2.5. Membrane Configuration

Membrane configuration is the geometry of the membrane and its position in space in relation to the flow of the feed and permeate (Berk, 2009). The desired characteristics of a

membrane configuration include compactness (i.e., the capability of packing as much membrane surface as possible into a module), low resistance to tangential flow (i.e., low friction and energy consumption, low pressure drop along the retentate flow channel), uniform velocity distribution, easy cleaning and maintenance, and low cost per unit membrane area (Berk, 2009). Different types of membrane configurations are flat-sheet, tubular, and hollow fiber (HF). Flat-sheet membranes may be wrapped into spiral-wound modules or used in a plate-and-frame configuration, both of which are common in membrane-based systems. In the spiral-wound configuration, two large sheets of membrane are heat-sealed on three sides and create a bag. A flexible spacer mesh or a porous support layer is inserted into the bag and forms a free space between the two membranes for permeate flow. The assembly is spirally wound and forms a cylindrical module. This type of membrane has high packing density which is 492-1247 m^2/m^3 and has high potential for fouling with difficult cleaning and moderate cost of manufacturing (Obotey Ezugbe & Rathilal, 2020). The plate-and-frame membranes are square and circular, arranged in vertical or horizontal stacks. These membranes cannot withstand very high pressure and are limited to MF and UF. The surface area to volume ratio of plate-and-frame modules and the packing density is not high (i.e., packing density: 148-492 m^2/m^3) (Berk, 2009). They have high manufacturing cost and moderate potential for fouling (Obotey Ezugbe & Rathilal, 2020). The tubular membranes are hollow tubes and have membranes located on their surface. The tubes function as a supporting structure that has high porosity (Berk, 2009). Their packing density is 20-374 m^2/m^3 and it has a low potential for membrane fouling (Obotey Ezugbe & Rathilal, 2020). HF modules are made up of hundreds to thousands of fibers (Judd, 2010). They are more common due to their

advantages of higher packing density (i.e., packing density: 492-4924 m^2/m^3), higher membrane area per cubic meter of module bulk volume, and low cost of manufacturing. These membranes are capable of inducing movement by mechanisms such as bubbling, and have the feasibility of backwashing; therefore, membrane fouling is reduced (Akhondi et al., 2017; Obotey Ezugbe & Rathilal, 2020).

2.2.6. Membrane Operation Mode

Two major flow modes of membrane process are dead-end and crossflow filtration as shown in Figure 2.1(a-b). The retentate accumulates on the membrane during dead-end filtration, but during crossflow filtration, the permeate moves across membrane pores, and the concentrated retentate flows away throughout the membrane (Dickhout et al., 2017). Both flow configurations have their own set of benefits and drawbacks. The key drawbacks of dead-end filtration are substantial fouling and concentration polarization, demanding periodic interruptions of the process to clean or replace the membrane on a regular basis (De Morais Coutinho et al., 2009). In crossflow filtration, liquid flow is parallel to a membrane surface and pressure drop leads the suspended particles to be transferred across the membrane surface by permeate flow; this operation mitigates cake layer formation on the membrane surface (Akhondi et al., 2017).

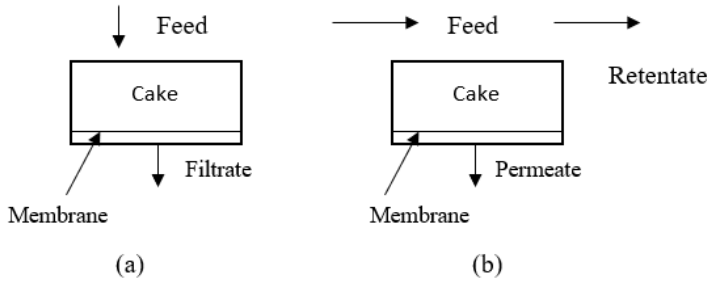

Figure 2.1 (a) Dead-end filtration (b) crossflow filtration "adapted from (Judd, 2010)"

Two operational modes have been used for two types of filtration such as constant flux and constant TMP as shown in Figure 2.2 (a-b) (Behroozi & Ataabadi, 2021). Throughout constant TMP, a sudden and fast decrease in flux occurs due to a high initial flux which can lead particles to be deposited on the membrane surface (Figure 2.2a) and form a dense cake layer followed by a slow flux decrease until a steady-state flux is achieved (Hussain, 2019). During constant flux, membrane fouling is lower because the initial TMP is low, and then, increases linearly or exponentially during the filtration process and eventually, it can have a sharp increase of TMP (Figure 2.2b) (Field et al., 1995).

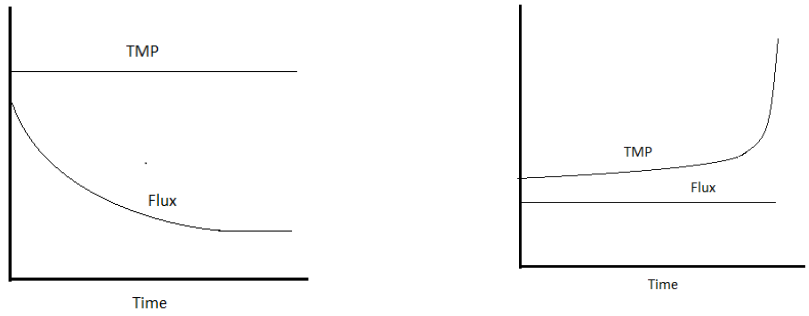

Figure 2.2 (a) Constant TMP mode (b) constant flux mode"adapted from (Hussain, 2019)"

2.3. Computational Fluid Dynamics (CFD)

In 1996, the first revolution in the simulation of the membrane process was fulfilled by Rautenbach for the hybrid distillation/pervaporation process (Rautenbach et al., 1996). They reported the advantages of using the process simulator, including physical property models and databases, simulation of the process with recycling loops, and performing sensitivity analysis. Then, researchers found other benefits from simulation tools such as estimating the material and energy balance for the whole process (Cao & Mujtaba, 2015), calculating parameters of the membrane by reducing the deviation of the model predictions from experimental data (Marriott & Sørensen, 2003), simulating, design, and optimizing of the whole process instead of a single membrane module (Ahmad et al., 2012), and decreasing experimental runs by the design of experiments (Galvanin et al., 2016). Therefore, there is a wide scope to enhance the use of simulation tools through chemical process in industry and academia.

CFD is one of the engineering systems utilizing mathematical modeling and numerical methods to investigate fluid flow challenges. The fundamental of CFD is based on the Navier-Stokes equations, explaining the fluid motion. The main benefit of CFD is being a reasonably priced technique to predict fluid flow and flow patterns without facing challenges of conducting a lot of experiments (Hussain, 2019). CFD speeds up process development, accelerates optimization of processes, and saves energy; therefore, it can be a promising approach to study different aspects of membrane filtration technology (Hussain, 2019). In this section, fundamentals of CFD modeling such as governing equations, initial and boundary conditions, and the applied methods have been discussed. Then, the application of CFD in membrane filtration technology and the related previous studies have been reviewed. Knowledge gaps and research hypothesis have been mentioned in the last section of this chapter.

2.3.1. Governing Equations

Continuity, momentum, and energy equations are the fundamental governing equations for fluid dynamics (Wendt et al., 2008). The conservation of mass and conservation of momentum (the Newton's second law) are explained by Eqs. (2.7) and (2.8), respectively (Fimbres-Weihs & Wiley, 2010).

$$\frac{\partial p}{\partial t} + \nabla \cdot (\rho u) = 0 \tag{2.7}$$

$$\frac{\partial (\rho u)}{\partial t} + \nabla . (\rho u u) = -\nabla p + \mu \nabla^2 u + \rho f \tag{2.8}$$

where ρ is the density of the fluid (kg/m^3), u is the fluid velocity (m/s), μ is the fluid viscosity (Pa·s), p is the pressure (Pa), t is time (s), and f is body forces per unit volume (m/s^2) (Ghidossi et al., 2006a; Blazek, 2015). Eq. (2.7) is a partial differential equation (PDE) type of the continuity equation. For an incompressible fluid (i.e., fluid whose volume or density does not change with pressure), the first term in Eq. (2.7) becomes zero and Eq. (2.9) can be written as follows.

$$\frac{\partial u}{\partial x} = 0 \tag{2.9}$$

Eq. (2.8) (i.e., Navier-Stokes equation) is the description of the fluid flow for incompressible Newtonian fluid (i.e., the fluid with constant viscosity, and shear rate in this type of fluid is in direct proportion to shear stress) with considering the impact of fluid viscosity. For inviscid flow (i.e., the flow of the fluid with no viscosity), the dissipative transport phenomena of viscosity, mass diffusion, and thermal conductivity are negligible and the Euler equations (Eq. (2.10)) are used (Anderson, 1995).

$$\frac{\partial(\rho u)}{\partial t} + \nabla \cdot (\rho uu) = -\nabla p + \rho f \tag{2.10}$$

Eq. (2.8) is also mentioned in a more general type by the conservation law of all fluid flow, as shown in Eq. (2.11) (Fasihi et al., 2012).

$$\frac{\partial(\rho \phi)}{\partial t} + div(\rho u \phi) = div(\Gamma_\phi grad\, \phi) + S_\phi \tag{2.11}$$

where ø is a dependent variable and can be either scalar or vector. When ø is 1, the conservation of mass equation can be derived. When ø is equal to u, the equation is for the momentum conservation. Temperature and concentration of the fluid can be used as ø and

applied for heat and mass transport, respectively. $\Gamma_{ø}$ is a suitable coefficient for ø, this coefficient is calculated by $\Gamma_{ø} = \rho D$ (D is diffusion coefficient) in mass transport equation and $S_{ø}$ is the source term (Cao, 2016). The actual type of conservation equation (integral form) is solved by CFD and is shown in Eq. (2.12).

$$\frac{\partial}{\partial t}\int_{CV} \rho\phi dV + \int_{A} n.(\rho u\phi)dA = \int_{A} n\cdot(\Gamma_{\phi} grad\phi)dA + \int_{CV} S_{\phi}dV \tag{2.12}$$

Transport equation is stated as the most generated and integrated form for time-dependent problems as shown in Eq. (2.13) (Cao, 2016).

$$\int_{\Delta t}\frac{\partial}{\partial t}\int_{CV} \rho\phi dV + \int_{\Delta t}\int_{A} n\cdot(\rho u\phi)dA = \int_{\Delta t}\int_{A} n\cdot(\Gamma_{\phi} grad\phi)dA + \int_{\Delta t}\int_{CV} S_{\phi}dV \tag{2.13}$$

where *CV* is control volume, *V* is volume, *A* is area, and *t* is time.

2.3.2. Initial and Boundary Conditions

A set of constraints to identify the solution of simulations are expressed as the initial and boundary conditions which are divided into three types based on the mathematical viewpoint; Dirichlet boundary conditions, Neumann boundary conditions, and Cauchy boundary conditions. Dirichlet boundary conditions specify the values of variables, whereas Neumann boundary gives values to the derivatives of variables at the boundaries. Cauchy boundary conditions identify the function values and the derivatives of variables at the boundaries. When boundary condition is wrongly used, it causes imprecise simulation and adversely affects the stability and the convergence speed (Pozrikidis, 2009; Cao, 2016).

2.3.3. Numerical Methods

Different numerical discretization approaches such as finite difference methods (FDM), finite element methods (FEM), and finite volume methods (FVM) have been used to solve PDEs that govern fluid flow (Keir & Jegatheesan, 2014). Table 2.1 shows the summarized explanation for each method (Keir & Jegatheesan, 2014; Cao, 2016). COMSOL Multiphysics interfaces use FEM to solve the constituent PDEs in an integral form. Unknowns are discretized as sums over a set of basic functions defined on finite elements, rather than by discretization of derivatives on a grid of points. The finite elements are assembled by creating a mesh, which is a tessellation on the geometry with triangles in 2D or tetrahedra in 3D. The main benefits of the FEM over the FDM are its adaptability to the complicated geometries and the simplicity of handling discontinuous gradients of a variable (Dickinson et al., 2014).

Table 2.1 Summary of discretization approaches (Keir & Jegatheesan, 2014; Cao, 2016)

Method	Base	Formulation	Mesh	Boundary Condition
FDM	• Taylor series expansion (The differential form of the conservation equations)	• Easy to be conceptually formulated	• Must be in two or three dimensions • Curvilinear meshes should be transferred to structured Cartesian coordinates • More challenging to adjust complicated geometries	• Neumann boundary conditions (i.e., derivatives of variables defined at boundaries) cannot be exactly imposed, only approximated
FEM	• The integral form of the conservation equations	• Less straight forward	• Easier to adjust complicated geometries • Possible to use non-Cartesian coordinates and unstructured meshes	• Neumann boundary conditions are precisely imposed.
FVM	• The integral form of the conservation equations	• Able to be formulated according to FEM or FDM	• Depends on formulation (FEM or FDM)	• Neumann boundary conditions are precisely imposed.

2.4. Application of CFD to Model Membrane Filtration Technology

2.4.1. Simulating Free Flow

Early simulation studies modeled free flow in channels with porous walls under laminar conditions to model the phenomena taking place inside membrane modules (Berman,

1953; Wah, 1964). Following that, Friedman & Gillis (1967) added the fluid viscosity to the computations to improve the model precision. The development of these models resulted in the investigation of laminar flow in a porous pipe with variable wall suction or variable radial mass flux. The applied method was solving the Navier–Stokes and continuity equations for a 2D or 3D steady and laminar flow of an incompressible homogeneous and Newtonian fluid with the maximum accuracy (Ghidossi et al., 2006b). Nassehi (1998) studied a technique to link the free flow model using the Navier–Stokes equations to the flow that passed through the membrane explained by the Darcy equation. This research was the initial step in establishing a complete model to decrease membrane fouling. Similarly, other studies suggested a model for the concentration polarization phenomenon along the membrane under different operating conditions (Damak et al., 2004, 2005). Since then numerical simulation has been found useful to improve the mass transfer correlation in the membrane modules (Ghidossi, et al., 2006b). It was found that these studies are ground-breaking to model the fluid flow in the membrane processes under laminar conditions. The reported models have provided an opportunity to simplify existing theories and better understand the involved phenomena. In the following section, the simulation of oily wastewater as a two-phase fluid flowing along the membrane module has been specifically reviewed.

2.4.2. Simulating Oily Wastewater Transfer

In a system containing multiple phases, when a phase is distributed in another phase in a shape of small droplets, it will be complex to follow the interface of these droplets. Oily wastewater is an oil-in-water emulsion in which the droplets of oil are very small and are

dispersed in the water phase. Therefore, it is challenging to use CFD in order to investigate the transport of oily wastewater in membrane filtration technology (Zoubeik, 2018). These challenges include coupling fluid continuum and the membrane porous medium continuum since continua of fluid and porous media have various length scales, and variables are linked differently. In real-world applications, specific oil percentage passes through the membrane, and finding a suitable framework explaining the real permeate quality is another challenge in modeling of the permeation process. To address these challenges, previous studies used two techniques to investigate the transport of oily wastewater through the membrane module in CFD: (a) a micro-structure CFD modeling integrated with investigation of a single/multiple oil droplet movement inside the membrane pores, (b) assuming the membrane as a boundary section and simulating the concentration polarization (Zoubeik, 2018).

In micro-scale investigations, the behavior of the oil droplets reaching the membrane has been studied through two factors; the threshold capillary pressure at which the droplet could pass through pores of the membrane and the CFV that moved the droplet off the membrane. As an example, Darvishzadeh & Priezjev (2012) conducted a numerical simulation using Navier–Stokes equation to study the effect of TMP and CFV on the entry dynamics of thin oil films and droplets of oil into the pores of various cross sections. They performed a comprehensive investigation of the oil droplet dynamics close to the pore entry in three different zones. Results showed that increase in CFV led the oil droplet to be deformed close to the entrance of the membrane pore and this increased the critical pressure of permeation. They also demonstrated a phase diagram for rejection, permeation, and breakup of oil droplets which were dependent on TMP and shear rate.

In addition, most previous studies investigated the impact of cake layer formation and concentration polarization on the performance of membrane and membrane flux when membrane was treating oily wastewater under the constant TMP. For example, Zare et al. (2013) performed a 2D CFD modeling in the MF technology to treat oily wastewater. They studied the impacts of Re on concentration polarization and oil concentration. Based on the results, increase in membrane flux occurred at higher TMP and Re, and lower feed concentration. However, their model could not predict the layer of concentration polarization accurately because they overlooked the interactions among droplets of oil and surface of the membrane and also the inter particle interactions of oil droplets. Asadi Tashvigh et al. (2015) carried out a study to predict the decrease of membrane flux in MF containing oily wastewater. To describe back-diffusion of oil droplets from the membrane surface to the bulk, a combination of molecular and shear-induced diffusion coefficient was used. The impacts of TMP and CFV on the precision of the model and various operational conditions on concentration polarization layer were investigated. They assumed 100% of rejection for filtration process and their model was capable to precisely predict the trend of membrane flux with time compared to previous studies. However, these studies did not consider pore blocking in their modeling approach. Behroozi et al. (2019) suggested a 2D CFD modeling to simulate pore blocking in the MF process and filled the knowlegde gap. Their study improved the precision of prediction about 15%. Results showed that with increasing inlet oil concentration from 1000 to 10000 mg/L, the maximum value of oil concentration on the membrane surface increased 9.68 times. In addition, the increase in CFV from 0.5 to 1.1 m/s caused the maximum thickness of concentration polarization layer to decrease 14%. These numerical studies provided

information about the membrane performance when the oily wastewater passes through the membrane module to investigate its impact on membrane fouling, concentration polarization, and flux decline under the constant TMP using a 2D CFD modeling.

2.4.3. Simulating Hydrodynamic Conditions

CFD has been used to determine, explain, and optimize the complicated hydrodynamics of membrane filtration systems generated by aerators, spacers, and geometry (Smith et al., 2002; Tarabara & Wiesner, 2003; Koutsou et al., 2004; Cachaza et al., 2009; Bucs et al., 2015; Karpinska & Bridgeman, 2018; Kim & Chung, 2019; Wang et al., 2021). One of the main hydrodynamic technique to reduce particle deposition on the membrane surface is bubbling, leading to an unsteady-state condition of shear at the surface of the membrane through turbulent eddies, fiber oscillations, particle scouring, and the recirculation of the reactor liquid (Akhondi et al., 2017). When aeration is added to the membrane filtration system, a gas-liquid two-phase flow should be considered in a model to generate hydrodynamic instabilities in the system affecting concentration polarization and sweeping away cake layer (Wibisono et al., 2014). This leads to increasing the membrane flux and improving the membrane performance under the constant TMP. This idea was developed by Smith et al. (2002), they simulated the role of aeration in UF process to understand and quantify membrane flux enhancement due to gas sparging. Their results showed that the flux enhancement was related to the increase in the mass transfer coefficient. Khalili-Garakani et al. (2011) studied the impact of aeration flow rate on shear stress in a bench-scale MBR and showed that the average shear stress on the surface of the membrane increased by increasing aeration flow rate. They reported that a better distribution of shear

stress was found by a homogenous distribution of air on the surface of the membrane. In addition, they reported that when the baffle angle in membrane tank changed from 90° to 85°, the shear stress increased and membrane fouling decreased. This study showed that membrane fouling and membrane flux had a close relationship with the shear stress on the surface of the membrane and they were related to the shear stress of air and liquid flows. Similar studies investigated the hydrodynamics of MBR process at large scales, hydrodynamic characteristics of a full-scale MBR for municipal wastewater, and evaluated the mixing and energy of MBRs with different configurations (Kang et al., 2008; Wang et al., 2009; Amini et al., 2013). Yan et al. (2016) investigated the hydrodynamic behavior in a bench-scale MBR. They showed that the average shear stress was related to the aeration intensity and affected membrane fouling. They also mentioned that geometrical characteristics affected the hydrodynamics of an MBR, which was directly related to membrane fouling rate. Kim & Chung (2019) analyzed velocity distribution, shear stress between the membranes and baffle, and shear stress between the membranes in a bench-scale membrane reactor. The results were validated by video imaging to capture the bubble pattern. The shear stress between the membrane and the baffle ranged from 0 Pa to 0.1 Pa at the 1/3 point from the bottom of the membrane module. This study also showed that the fluid velocities and the membrane surface shear stresses in the vicinity of membranes significantly affected membrane fouling. Recently, Wang et al. (2021) suggested a new aerator design for a free bubbling process in a bench-scale MBR. Simulations indicated that an aerator with an additional side nozzle was optimized to generate beneficial hydrodynamics. They used the aerator in a large-scale MBR with plate dimensions of 1800 mm×490 mm×6 mm (L×W×H) with low energy consumption. The majority of the studies

did not evaluate the effect of aeration on hydrodynamic behavior of a pilot-scale membrane filtration system containing various types of oily wastewater without using biological processes.

2.4.4. Simulating Treatment Process and Scale-up

Previous studies used CFD to provide an understanding into the phenomena taking place inside the membrane modules (Damak et al., 2004, 2005; Parvareh et al., 2011; Keir & Jegatheesan, 2014; Bucs et al., 2014; Saeed et al., 2015; Completo et al., 2016; Ren et al., 2020) and to improve the overall performance of this technology (Cortés-Juan et al., 2011; Saeed et al., 2012; Lotfiyan et al., 2014; Wang et al., 2019). In addition, studies simulated membrane filtration technology for treatment purposes; Vinther et al. (2014) simulated the UF process for dextran filtration using COMSOL Multiphysics based on the FEM. The model explained the flow of fluid and filtration process in HF membranes by solving the Navier–Stokes equation along with the continuity equation for both the solute and the solvent. The model was validated with experimental results of concentration in the permeate with a total error of less than 10^{-3}. This model was capable of simulating velocity field, the concentration field, and the pressure field in the bulk solution of an HF tube. The impact of different factors such as inlet velocity, molecular weight, and TMP on removal efficiency was investigated. However, the modeling results showed higher concentration in the permeate compared to the experiments. The issue was due to a parameter that was assumed as a constant concentration on the surface of the membrane. This assumption was not acceptable and this parameter should have been fitted to each specific experiment. Maarefian et al. (2017) simulated the removal of COD in a bench-scale HF-MBR to treat

high saline refinery wastewater using 2D CFD. This model explained the diffusion in the axial and radial directions of HF along with the momentum transfer toward the tube and shell. It was validated by COD concentration in the permeate achieved by experimental results. The velocity and concentration profiles were evaluated to investigate the effect of operating parameters in removing COD. The simulation results showed that the model had 7.35% relative error compared to the experimental results. However, previous modeling studies did not provide a comprehensive investigation of the membrane filtration system treating oily wastewater in pilot- and full-scale applications. In addition to investigating filtration, different CFD studies have upscaled the system. In membrane filtration, larger system dimensions (i.e., higher membrane surface area) lead to a higher treatment capacity as a result of the increase in the number of treatment sites (Mukherjee et al., 2016). Mukherjee et al. (2019) used equations of continuity, momentum, and convective-diffusive-adsorption based solute transport for filtration through HF module. The governing equations were solved using FEM by COMSOL Multiphysics. The model parameters were evaluated using the experimental results associated with long-term filtration of synthetic chromium (VI) solution. The model predicted the long-term performance of the system in terms of throughput and removal efficiency of chromium (VI). The validated model was further used for simulation of a large-scale membrane with high breakthrough volume interrelating number and length of fibers with the operating conditions such as TMP and crossflow rate (CFR). Recently, an MBR containing two tanks such as an aerobic tank (i.e., a tank in which the biochemical reactions happen) and a membrane tank (i.e., a tank in which the final filtration takes place) to treat oily wastewater was simulated and upscaled. A mathematical model was developed to define reaction and

mass transport inside the MBR using COMSOL Multiphysics. The model was used to recognize the most favorable design and operation conditions for the degradation of oil and grease. This numerical simulation provided an appropriate understanding of the involved mass transport mechanisms in the membrane tank; this was obtained by predicting fluid velocity and the dynamics of the total mass flux and concentration in the tank with the relative error of less than 2%. This study was only useful for biological-based membrane filtration systems and considered the sludge rheology and the reaction between the solutes and microorganisms to treat oily wastewater (Sánchez-Vargas & Valdés-Parada, 2021).

2.5. Knowledge Gaps and Research Hypothesis

Section 2.4 provided a comprehensive literature review about CFD modeling from simulating free flow to treatment process and scale up a membrane filtration system. Although different numerical research has been conducted on membrane filtration process, little information could be found simulating treatment of oily wastewater in a pilot- and/or large-scale membrane filtration system under the constant flux using 3D CFD modeling. The influence of aeration on the membrane fouling and identification of mechanism and hydrodynamic behaviour inside the pilot-scale membrane filtration systems containing two types of oily wastewater are other areas which has yet to be explored in detail. As a result, in this thesis the efficiency of oily wastewater treatment in a pilot-scale membrane filtration system under the constant flux using a 3D CFD modeling was investigated. In addition, the impact of aeration on membrane fouling and TMP changes was studied. The mechanism and hydrodynamic behaviour of the system as a result of aeration were also

identified. Finally, the validated model was used for scale-up to explore the capability of the system in a large-scale field application. The following chapter outlines the research methodology, which was implemented to address the research gaps.

CHAPTER 3 RESEARCH METHODS

3.1. Experimental Setup

The pilot-scale membrane filtration system consists of a membrane tank as shown in Figure 3.1 (a-b) containing two hydrophilic PTFE-HF membranes. Air (gas phase) was provided through air diffusers promoting mixing inside the tank and decreasing membrane fouling. Aeration flow rates were considered at 4, 4.8, and 6 m^3/h in various experimental runs. The synthetic oily wastewater was transferred to the membrane tank after being emulsified by a high-shear vertical mixer and it was considered a liquid phase in the modeling. Oily wastewater came in through the feed pump with a flow rate of 1500 L/h to the membrane tank to penetrate through the membranes where the filtration process happened and yielded a permeate flow of treated water. The filtration was conducted under the constant flux (i.e., in the range of 6 and 12 $L/m^2 \cdot h$) (Keyvan Hosseini et al., 2023). The permeate flow rate was calculated based on the membrane surface area of two membranes which is 12 m^2 (i.e., 72 and 144 L/h). The oil concentrations in the inlet of the membrane tank were 50 and 100 mg/L.

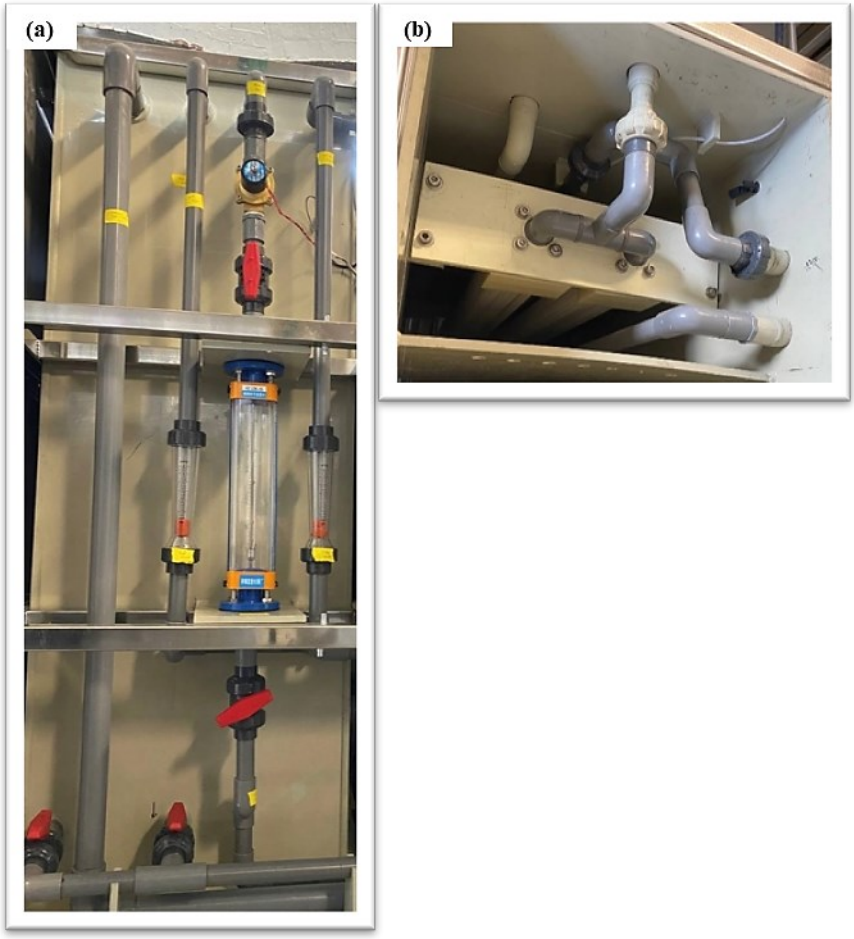

Figure 3.1 (a) Exterior view and (b) interior view of the membrane tank

3.2. Analytical Methods

In this study, the concentration of oil in the effluent was analyzed using an ultraviolet-visible (UV-Vis) spectrometry according to the methodology described in Zheng et al. (2015). The dynamic viscosity was measured by ASTM D7042 during the experimental runs. TMP as a function of the resistance of a fouling layer (Hussain, 2019) was monitored and recorded using a programable logic controller (PLC) (WE!NVIEW, China) during each run.

3.3. Theoretical Descriptions

A 3D CFD model for the membrane system treating oily wastewater was developed utilizing COMSOL Multiphysics® (Version 6, COMSOL Inc.). Based on the dimensions of the experimental pilot unit, the 3D geometry of the model was designed for implementing the main governing equations. Proper boundary conditions were identified and mesh independence analysis was conducted. The developed model was then validated using available experimental data in corresponding conditions. The comprehensive model development procedures are explained in the following sections.

3.3.1. Geometry Design

Figure 3.2 shows the elements of the model geometry designed for the 3D CFD model, wherein the computational region is a rectangular geometry and has a dimension of 1.525 m × 0.564 m × 0.4 m (H × L × W). The length, width, and height of each membrane module are 0.16 m × 0.14 m × 1.295 m, respectively. The packing of fibers in each HF membrane was considered a porous membrane module (Wang et al., 2010; Cai et al., 2016). The aeration system has 10 aerator pores at the bottom of the membrane tank to provide air bubbles in the membrane filtration system and the distance between aerator and the bottom of the membrane module is 98 mm.

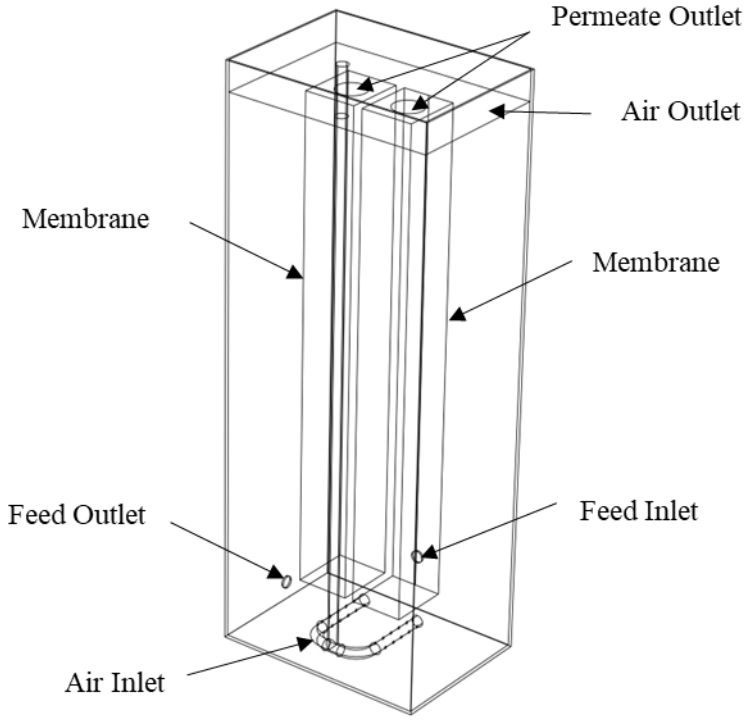

Figure 3.2 3D geometry design in the CFD modeling

The assumptions of the model are summarized as follows:

- The solution in the membrane tank was completely mixed and the concentration, viscosity, and density were constant.
- The differential pressure among the membranes did not lead to any variation in the membranes' physical characteristics.
- The pore structure of the membrane support was homogeneous and isotropic.
- Flow through the membrane tank and inside porous membranes was laminar, incompressible, and isotropic.

- The liquid was assumed to be Newtonian and in this type of fluid the shear stress is directly proportional to the shear rate at a fixed temperature and pressure. Newton's law of viscosity defines the relation between shear stress and the rate of deformation which is expressed in Eq. (3.1)

$$\tau = -\mu_d \frac{du_x}{dy} = \mu(y) \tag{3.1}$$

where τ is the shear stress (Pa), μ_d is the dynamic viscosity (Pa·s), and $\frac{du_x}{dy}$ or Y is the shear rate (1/s) (Islam & Hossain, 2021). The shear rate was measured by CFD in this study.

3.3.2. Operational and Geometrical Parameters

In this study, CLD as heavy crude oil and VLSFO as light crude oil were used. Properties of crude oils are reported in Table 3.1 according to the experiments and previous studies (Hamam et al., 1988; Mueller et al., 1997; Zheng & Price, 2012; Wang et al., 2014; Fang et al., 2015; Ebrahimi et al., 2015; The Pennsylvania State University, 2020).

Table 3.1 Physical properties of two types of oils

Parameter	CLD	VLSFO
Dynamic Viscosity of Oil (25°C) (Pa·s)	0.331	0.0104
Density of Oil (25°C) (g/cm^3)	0.926	0.877
API (°)	21.8	29.7
Diffusion Coefficient of Oil in Water (m^2/s)	8.9444e-9	1.1111e-8
Diffusion Coefficient of Oil in Membrane (m^2/s)	3.298e-16	1.2817e-14

The characteristics of oily wastewater are shown in Table 3.2. Oil droplet size analysis (i.e., using Mastersizer, United Kingdom) showed that the oil droplet size was less than 10 μm, and therefore, oily wastewater is considered stable (Chakrabarty et al., 2008). Table 3.3 shows the properties of the HF membranes (Sumitomo Electric, Japan) which were considered in the simulation.

Table 3.2 Oily wastewater characteristics at 23 °C

Oil Type	Oil Concentration (mg/L)	Viscosity (Pa·s)	Density (g/cm^3)
CLD	50	0.0009989	1.02
	100	0.001044	1.02
VLSFO	50	0.0009943	1.02
	100	0.0009970	1.02

Table 3.3 Properties of membranes (POREFLON^{TM} Module SPMW-11B6)

Material	Hydrophilic PTFE-HF Membrane
Porosity	0.83
Permeability	1.36e-10 m^2
Nominal Pore Size	0.08 μm (UF)
Membrane Area	6 m^2
PTFE Density	2.16 g/cm^3

3.3.3. Fluid Flow Modeling in the Membrane Tank

To obtain the concentration profiles in the membrane tank and membranes, the fluid velocity field is determined. The Navier-Stokes equation is used to model the flow of liquids with dispersed bubbles at low and moderate Re (Judd, 2010; Vera & Ruiz, 2012). In this model, the Navier-Stokes equation was used for the liquid phase to govern the oily wastewater motion in the membrane tank and it is seen as Newton's second law of motion for fluids (Konstantinos Dionysios, 2015) and the velocity of the bubbles is guided by a

slip model. A transport equation for the effective gas density was solved to achieve the volume fraction of bubbles. Momentum and continuity equations for liquid are shown in Eqs. (3.2) and (3.3), respectively. Eqs. (3.4) and (3.5) show a transport equation for the volume fraction of gas where (m_{gl}) is the mass transfer rate from gas to liquid (Al-Abbasi & Shams, 2019).

$$\rho_l \frac{\partial u_l}{\partial t} + \rho_l (u_l \cdot \nabla) u_l = \nabla \cdot \left[-pl + (\mu_l (\nabla u_l + (\nabla u_l)^T)) \right] + \phi_l \rho_l g + F \tag{3.2}$$

$$\rho_l \nabla \cdot u_l = 0 \tag{3.3}$$

$$\nabla \cdot (\phi_g \rho_g u_g) = -m_{gl} \tag{3.4}$$

$$\phi_g \rho_g = \rho_{g,eff} \tag{3.5}$$

where the indices *l* and *g* refer to the liquid and gas phases, respectively. The volume fractions of each phase are denoted by ø. u_l is the fluid velocity, *p* is the fluid pressure, ρ_l is the fluid density, and μ_l is the fluid dynamic viscosity. In Eq. (3.2) terms correspond to the inertial forces (first and second terms), pressure forces (third), viscous forces (fourth), and external forces applied to the fluid (fifth and sixth). Eq. (3.2) was solved by the continuity equations for the liquid phase (Eq. (3.3)) and momentum equations for the gas phase (Eqs. (3.4) and (3.5)) (Konstantinos Dionysios, 2015). In Eq. (3.4), $\phi_g \rho_g \mu_g$ is associated with the convection term of gas phase and $\phi_g \rho_g$ is effective gas density.

The difference between gas velocity and liquid velocity is slip velocity (Eq. (3.6)). The slip velocity was calculated by pressure-drag balance. As a result of buoyancy, bubbles rise through a liquid in the membrane tank, and therefore, pressure forces balance the

viscous drag forces (f_D) on a gas bubble. The velocity between the two phases is governed by Eq. (3.7) and Eq. (3.8) (Hekmat et al., 2010). In this study, the average diameter of bubbles was assumed to be 4 mm, and hence, the drag coefficient (C_d) was solved by Eq. (3.9) which is based on Sokolichin, Eigenberger, and Lapin Model (Becker et al., 1994; Kuzmin & Turek, 2002). The surface tension used in the model was assumed to be negligible, because the radius of bubbles is large, meaning that the pressure difference inside and outside of the bubble is small (Zhang et al., 2015). Eq. (3.10) shows the Eotvos number (E_0) used in the drag coefficient equation and demonstrates the ratio of gravitational force and surface tension force (Muradoglu & Tasoglu, 2010) where σ is the surface tension coefficient and d_b is the bubble diameter.

$$u_g = u_l + u_{slip} \tag{3.6}$$

$$\phi_l \nabla \rho = f_D \tag{3.7}$$

$$f_D = -C_d \frac{3\rho_t}{4d_b} \left| u_{slip} \right| u_{slip} \tag{3.8}$$

$$C_d = \frac{0.622}{\frac{1}{E_0} + 0.235} \tag{3.9}$$

$$E_0 = \frac{g p_l d_b^2}{\sigma} \tag{3.10}$$

The initial velocity of the liquid in three dimensions is 0 m/s. The initial effective gas density is 0 kg/m^3 and the initial pressure is 0 Pa. The various gas and liquid boundary conditions are listed in Table 3.4. The feed flow rate is 1500 L/h and the fluid was assumed to be fully developed flow.

Table 3.4 Boundary conditions used for solving the momentum equation

Boundary Selection	Liquid Boundary Condition	Gas Boundary Condition	Equation
Air Inlet	No-Slip	Gas flux	$u_l.n = 0$ $-n.N_{\rho_g\phi_g} = N_{\rho_g\phi_g}$
Air Outlet	No-Slip	Gas Outlet (Outflow)	$u_l = 0$
Feed Inlet	Flow Rate	No Gas Flux	$-n.N_{\rho_g\phi_g} = 0$
Feed Outlet	Pressure	No Gas Flux	$[-\rho l + K]n = -\hat{p}_0 n$ $-n.N_{\rho_g\phi_g} = 0$

where n is the vector normal to the boundary, K is a term related to viscous force, u_l is fluid velocity, and $N_{\rho_g\phi_g}$ is the gas mass flux.

3.3.4. Fluid Flow Modeling in the Membrane Modules

The velocity of fluid flow in a membrane is governed by Darcy's law (Yeh et al., 2005). Eqs. (3.11) and (3.12) show the continuity and Darcy velocity equations, respectively in a membrane (Yeh et al., 2005).

$$\frac{\partial}{\partial t}(\varepsilon_p \rho) + \nabla \cdot (\rho u) = Q_m \tag{3.11}$$

$$u = -\frac{\kappa}{\mu}(\nabla p + \rho g) \tag{3.12}$$

where ε_p is membrane porosity, p is the pressure, μ and ρ are the fluid viscosity and density, respectively, g is the gravity acceleration, Q_m is the momentum source term, and κ is the membrane permeability. In addition, membrane flux is indicated by Eq. (2.5)

interrelating TMP, resistance, and fluid viscosity. In this study, resistance was affected by different operating parameters such as aeration flow rate, inlet oil concentration, permeate flow rate, and oily wastewater viscosity and measured based on experimental data (Jalilvand et al., 2014). Table 3.5 summarizes boundary conditions used in the modeling.

Table 3.5 Boundary conditions used for solving the membrane-related equation

Boundary	Boundary Selection	Liquid Boundary Condition	Equation
Inlet	Membrane Surface	Pressure	$p=p_0$
Outlet	Permeate Outlet	Permeate Velocity	$-n \cdot \rho u = -\rho u_0$

3.3.5. Mass Transfer in the Membrane Tank and Membrane Modules

In the membrane tank, Eq. (3.13) describes the oil concentration distribution in the membrane tank. The material balance in the membrane tank is explained using a momentum equation (Eq. (3.13)), where D_i is the diffusion coefficient of the oil in the water and u is the vector field explaining the flow velocity and c_i is the oil concentration in the tank. It includes the accumulation term (first term), diffusion term (second term), convection term (third term), and the adsorption and desorption rate (R_i) (fourth term) (Petersson, 2020).

$$\frac{\delta c_i}{\delta t} + \nabla(-D_i \nabla c_i) + u \cdot \nabla c_i = R_i \tag{3.13}$$

For the membrane module, the mass transfer of oil in the membrane is also described by convection and diffusion terms as shown in Eq. (3.14). In Eq. (3.14), $D_{D,i}$ and $D_{e,i}$ are the dispersion tensor and the effective diffusivity, respectively.

$$\frac{\partial(\varepsilon_p c_i)}{\partial t}+\frac{\partial(\rho c_{p,i})}{\partial t}-\nabla\cdot(D_{D,i}+D_{e,i})\nabla c_i+u\cdot\nabla c_i=R_i+S_i \tag{3.14}$$

To solve the mass transfer equations, inlet concentrations of oil for each run were used and boundary conditions are shown in Table 3.6.

Table 3.6 Boundary conditions for mass transfer equations

Boundary	Boundary Selection	Boundary Condition	Equation
Inlet 1	Feed Inlet	Concentration	$c_i = c_{0,i}$
Outlet 1	Feed Outlet	Outflow	$n.D_i\nabla c_i = 0$
Outlet 2	Permeate Outlet	Outflow	$n.D_i\nabla c_i = 0$

Hydrophilic or hydrophobic characteristics of the membrane and interfacial tension impacts, as a result of the interaction between membrane surface and oil droplets have been specified by capillary diffusion (Behroozi et al., 2019). In the present study, the contact angle between membrane surface and oil droplets is 122˚ which shows that the membrane is hydrophilic based on the manufacturing company. To consider the hydrophilicity of the membrane in this study, the term partition coefficient (K_{oil}) was added to the module of mass transfer which indicates the ratio between oil concentration inside the membrane and outside the membrane (Figure 3.3) shown in Eq. (3.15) (COMSOL, 2022).

$$K_{oil}=\frac{c_{oil\_inside}}{c_{oil\_outside}} \tag{3.15}$$

where C_{oil_inside} is the oil concentration inside the membrane, $C_{oil\_outside}$ is the oil concentration outside the membrane.

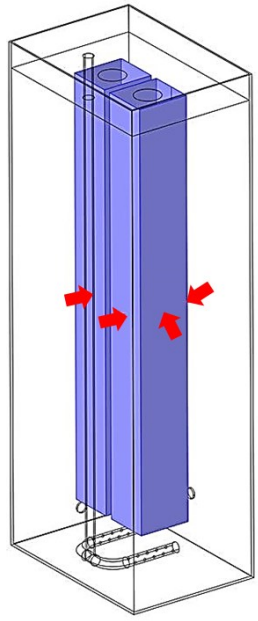

Figure 3.3 Specified regions related to partition coefficient on membrane boundaries

In this research project, the term partition coefficient was calculated based on the effluent oil concentration in various experimental conditions.

3.3.6. Upscaling Approach

Upscaling an oily wastewater treatment system using CFD simulation helps to successfully use the pilot-scale system for larger-scale applications. It is important that models are applicable at a larger-scale level because of the hierarchical nature of the system, and they should also be capable of capturing the essential information from the real current system (Sánchez-Vargas & Valdés-Parada, 2021). In this study, the derivation of mathematical models for the membrane filtration system based on the upscaling index was done. In this perspective, upscaling was used to indicate the systematic transferring of information from a specific scale level to a superior one (Sánchez-Vargas & Valdés-Parada, 2021). When

the current pilot-scale system was modeled and validated, it was used to upscale the oily wastewater filtration system. Upscaling index was defined as the ratio between the field throughput (10,000 L/h) and the maximum throughput of the current system (240 L/h). Eqs. (3.16) to (3.23) show the equations that were used to upscale the model. Throughout scale-up, based on the upscaling index, the volume of the membrane tank, number of the membrane modules and aerators were changed and simulated with the validated model.

As shown in following equations, some built-in mathematical functions in the software were used. One of them is ceil, which is the "nearest following integer" and mostly it is written as "ceil (x)". This function was used to set an upscaling index for the system (Eq. (3.16)). Also, this equation shows the number of units after upscaling based on the obtained ratio. Since the base of upscaling was a unit containing two membranes, number of units was multiplied by 2 to understand the number of membranes (Eq. (3.17)). Number of units in the x direction is shown in Eq. (3.18). The floor is another built-in mathematical function in the software. It is "nearest previous integer" and mostly it is written as "floor (x)". Eq. (3.19) was used to measure the number of units in the y direction. To calculate width, length, and height of the membrane tank, Eqs. (3.20) and (3.21) were used, respectively. Membrane tank height was the same as the current system which was 1.525 m. Total number of aerators and aeration flow rate are shown in Eqs. (3.22) and (3.23), respectively. Based on the upscaling index, the feed inlets and outlets in terms of number and location were designed. Figure 3.4 and Figure 3.5 show the upscaled system containing 42 units with 84 membranes. The entire upscaled system has a 1.525 m × 2.204 m× 1.936 m size (H × L × W) which can be easily used for larger-scale applications.

$$N_{unit} = ceil(\frac{Q_{field\_throughput}}{Q_{\max\_throughput(current\_system)}}) \quad (3.16)$$

$$N_{membrane} = 2 \times N_{unit} \quad (3.17)$$

$$N_{unit\_x} = ceil(sqrt(N_{unit})) \quad (3.18)$$

$$N_{unit\_y} = floor(sqrt(N_{unit})) \quad (3.19)$$

$$\mathrm{Tan}\, k_{width} = Mem_{width} \times N_{unit\_x} + 2 \times S_w + (N_{unit\_x} - 1) \times Mem_{distance} \times 4 \quad (3.20)$$

$$\mathrm{Tan}\, k_{length} = N_{unit\_y} \times 2 \times Mem_{depth} + (N_{unit\_y} \times 2 - 1) \times Mem_{distance} + 2 \times S_d \quad (3.21)$$

$$N_{aerator} = (N_{aerator\_y} \times N_{aerator\_x}) \times N_{unit\_y} \times 2 \times N_{unit\_x} \quad (3.22)$$

$$Q_{aeration\_upscaled} = Q_{aeration} \times N_{unit} \quad (3.23)$$

where $Q_{field\_throughput}$ is the required field throughput, $Q_{max\_throughput(current\_system)}$ is the maximum throughput of the current system, N_{unit} is total number of units, $N_{membrane}$ is total number of membranes, N_{unit_x} is the number of units in the x direction and N_{unit_y} is the number of units in the y direction, $Tank_{width}$ is the width of the membrane tank, $Tank_{length}$ is the length of the membrane tank, S_w is the side gap in the x direction, S_d is the side gap in the y direction, $Mem_{distance}$ is the distance between two membranes in a unit, Mem_{depth} is the depth of the membrane, Mem_{width} is the width of the membrane, $N_{aerator}$ is the total number of aerators, $N_{aerator\_x}$ is the number of aerators in the x direction and $N_{aerator\_y}$ is the number of aerators in the y direction. Also, $Q_{aeration\_upscaled}$ is the aeration flow rate in the upscaled system.

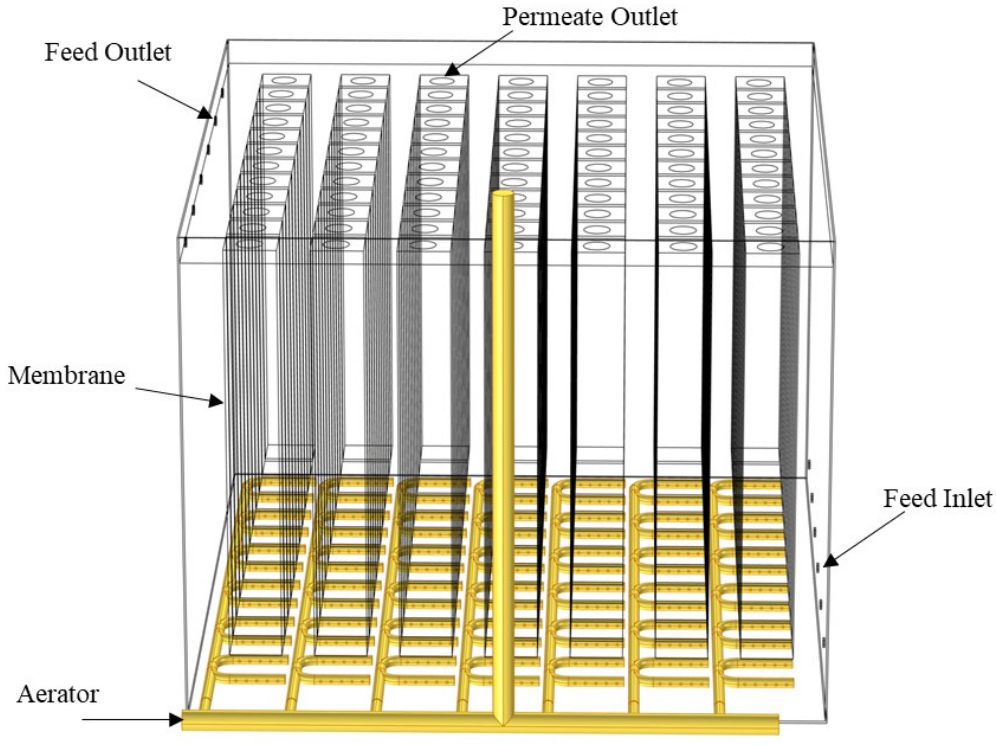

Figure 3.4 Geometry of the upscaled membrane filtration system from side view

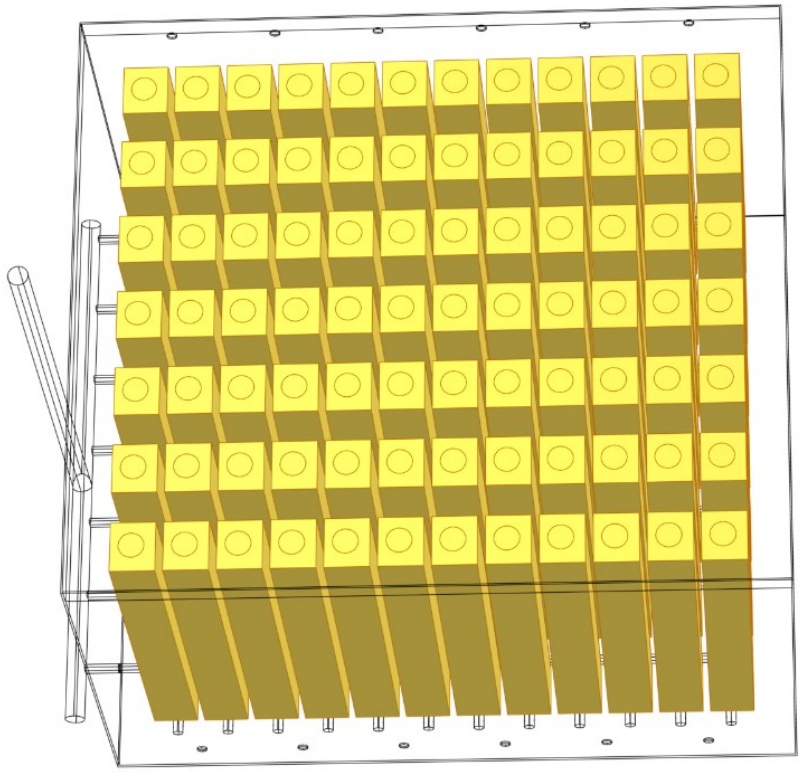

Figure 3.5 Geometry of the upscaled membrane filtration system from top view

3.3.7. Solution Methodology

The governing equations were solved by COMSOL Multiphysics 6 using the FEM and Figure 3.6 shows the flow chart for CFD simulation and numerical modeling. The fluid flow module was used to obtain the liquid and gas velocity distribution in the membrane tank. The first phase of this study was conducted at an unsteady-state condition for fluid flow module in the membrane tank to investigate the hydrodynamics of the system with the passage of time. Various CFD runs showed that fluid flow in the membrane tank reached a steady state at a short simulation time; therefore, to reduce computation time, this module was solved at a steady state in the second phase. The achieved velocity from this module was used in the mass transfer module. The velocity of the fluid in the membrane was estimated by Darcy's law in the membrane module and the achieved velocity was used in the porous media mass transfer module. After coupling three modules in three dimensions, the mass transfer module was solved in a time-dependent model, to understand the concentration of oil after the filtration process.

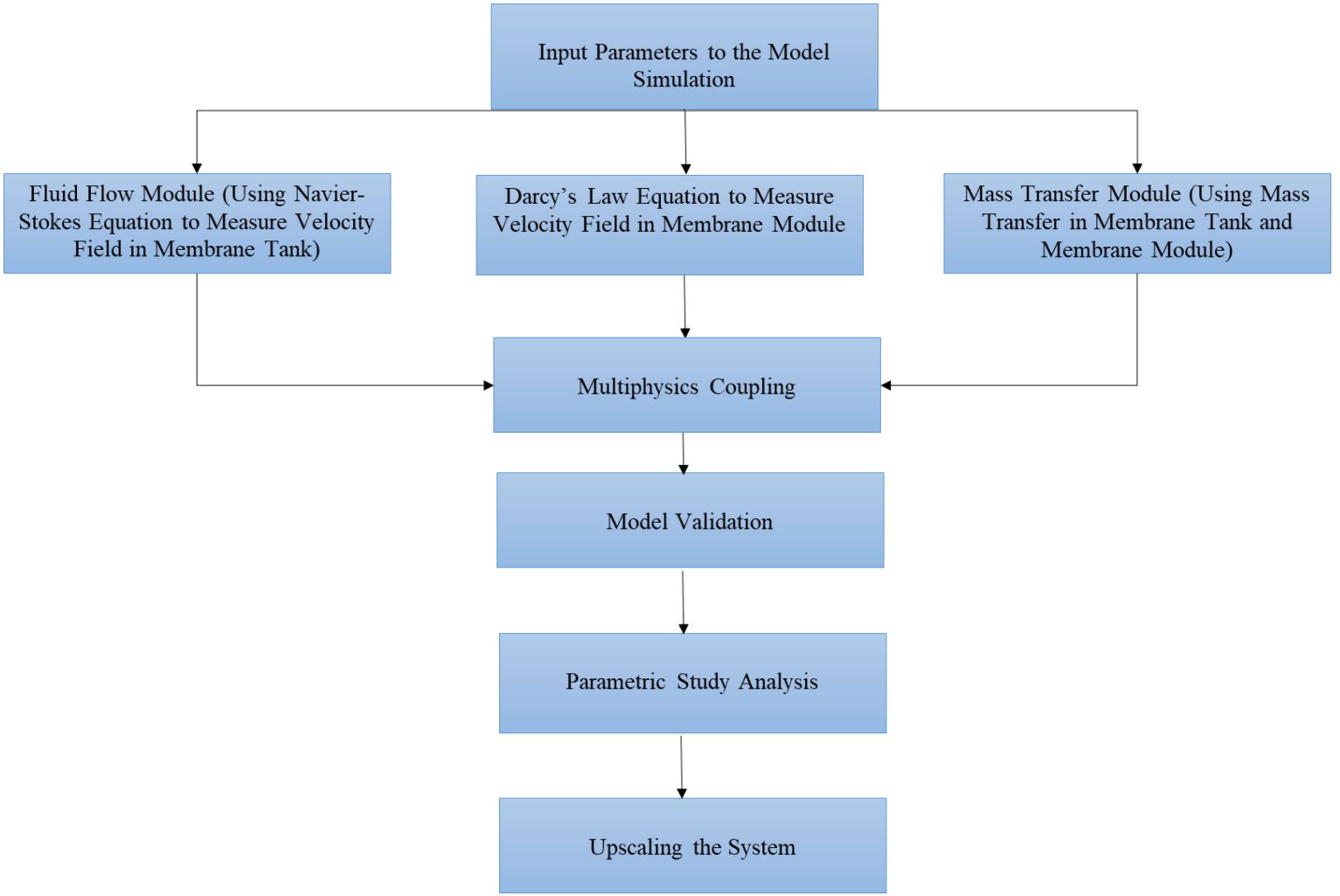

Figure 3.6 Flow chart of the CFD simulation and numerical modeling

3.4. Model Validation

3.4.1. Mesh Independence Analysis

In this CFD model, free tetrahedral geometry mesh configuration was used to generate meshes using a mesh controlling parameter (Madadi Avargani & Divband, 2022). The higher numbers of grids offered superior solution accuracy. To test the precision of the results and save computation time and cost, a grid independence study was conducted which estimated the optimum simulation grid size for the simulation domain (Jalilvand et al., 2014). Predicted oil concentration in the effluent was checked for various grid sizes and utilized as a criterion to check mesh independency. It was compared with the effluent oil concentration achieved by experiments which are shown in Table 3.7. A qualitative representation of the generated mesh for membrane tank simulation with HP® CORE i7 3.4GHz CPU and 16 GB of RAM is shown in Figure 3.7. The results reported in this study were obtained using a computational mesh for fluid dynamics with 396,364 domain elements. This mesh compared to finer meshes (476,414 domain elements), generated less than 2% average error in the results, which was adequately precise.

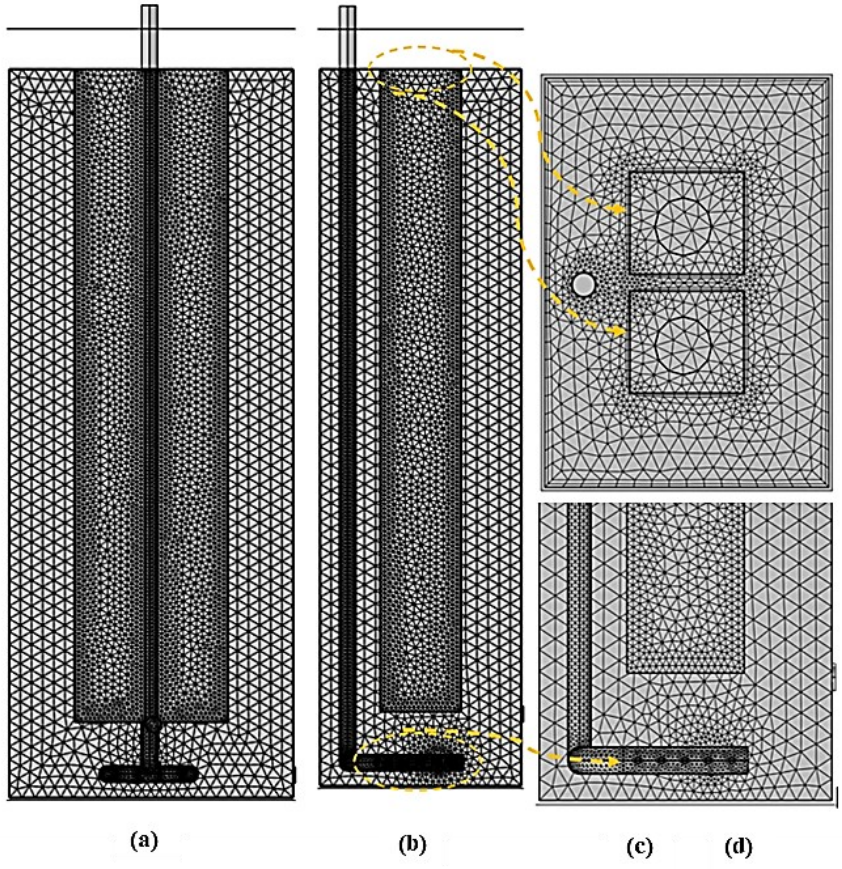

Figure 3.7 Qualitative representation of the generated mesh from (a) front view, (b) side view, (c) top view, and (d) side view magnifying the aeration section

Table 3.7 Results of mesh independence analysis

Test Samples	Domain Elements	Boundary Elements	Edge Elements	Relative Error (%)
1	276,625	66,086	2,415	7.87
2	342,530	78,734	2,606	5.95
3	**396,364**	**90,619**	**2,759**	**1.79**
4	476,414	104,373	2,918	1.65

3.4.2. Numerical Model Validation

Eq. (3.24) was used as a criterion for model validation using oil removal efficiency. The relative error (RE) is described in the following equation.

$$RE = \left| \frac{E_{oil,removal\_Exp} - E_{oil,removal\_Model}}{E_{oil,removal\_Exp}} \right| \times 100 \tag{3.24}$$

where $E_{oil,removal\_Exp}$ is oil removal efficiency achieved from experiments and $E_{oil,removal\_Model}$ is oil removal efficiency obtained from the model. In addition to validation with oil removal efficiency, average TMP was analyzed during the experimental runs and compared with simulation results as calculated by Eq. (3.25).

$$RE = \left| \frac{TMP_{Exp} - TMP_{Model}}{TMP_{Exp}} \right| \times 100 \tag{3.25}$$

where TMP_{Exp} is the average TMP achieved from experiments and TMP_{Model} is the average TMP achieved from the model. The relative errors in Table 3.8 for both oil removal efficiency and average TMP show that the simulation results have a good agreement with experimental data at various operating conditions with CLD and VLSFO; the errors were less than 5%. Hence, the proposed model is reliable and can be used for system parametric study.

Table 3.8 Results of numerical model validation with experimental data containing CLD and VLSFO (oil removal efficiency and average TMP)

Run	Type of Oil	Inlet Oil Concentration (mg/L)	Aeration Flow Rate (m^3/h)	Permeate Flow Rate (L/h)	Oil Removal Efficiency (Experiment) (%)	Oil Removal Efficiency (Model) (%)	RE (%)	TMP (Experiment) (kPa)	TMP (Model) (kPa)	RE (%)
1	CLD	50	4.8	72	98.91	98.90	0.010	2.75	2.88	4.73
2	CLD	50	6	72	94.48	94.62	0.148	2.53	2.61	3.16
3	CLD	50	4.8	144	96.87	97.02	0.155	3.14	3.26	3.82
4	CLD	50	6	144	90.68	90.38	0.332	2.99	2.99	0
5	CLD	100	4.8	72	98.06	98.16	0.102	3.47	3.63	4.61
6	CLD	100	6	144	91.19	90.75	0.483	3.5	3.66	4.57
Mean							**0.205**			**3.48**
7	VLSFO	50	4.8	72	98.97	99.02	0.051	2.55	2.61	2.35
8	VLSFO	50	4.8	144	98.94	98.92	0.020	2.89	2.98	3.11
9	VLSFO	100	4.8	72	99.11	99.15	0.040	3.23	3.37	4.33
Mean							**0.037**			**3.26**

CHAPTER 4 RESULTS AND DISCUSSION

4.1. Investigation of the System Hydrodynamics

Aeration is one of the effective physical cleaning approaches to scour the membrane and reduce membrane fouling, leading to the changes on hydrostatic pressure along the surface of the membrane and affecting the behavior of local filtration (Braak et al., 2011; Li et al., 2016; Bérubé, 2020). In this study, different hydrodynamic analyses have been conducted, and the impact of aeration on TMP was analyzed.

4.1.1. Impact of Aeration Flow Rate on Gas Volume Fraction in the Membrane Tank

In the present study, aeration flow rates were chosen in the range of 4.8, 6, and 6.8 m^3/h and were analyzed for two types of oily wastewater containing CLD and VLSFO. Figure 4.1 and Figure 4.2 show the changes in gas volume fraction based on numerical modeling at three aeration flow rates for two types of oily wastewater. The volume average operator was used to measure gas volume fraction in the membrane tank. In this system, gas entered the membrane tank from the aerators at the bottom of the membrane modules. As time passed, the profile grew and remained fixed after a while as shown in Figure 4.1 and Figure 4.2. Based on Figure 4.1, when oily wastewater contained 100 mg/L of CLD after 25 s at the aeration flow rate of 4.8 m^3/h and the permeate flow rate of 72 L/h, the average gas volume fraction was at about 2.50%, while at the same condition for VLSFO, it was at 2.52% (as shown in Figure 4.2). For CLD with the aeration rate of 6 m^3/h and the same permeate flow rate, the gas volume fraction reached 3.68% at 35 s, and then, had a stable

condition, while the fraction reached 3.8% at 35 s for VLSFO. The gas volume fraction obtained 5.4% and became steady for aeration flow rate of 6.8 m^3/h and the same permeate flow rate after 60 s for CLD, whereas the gas volume fraction reached 5.6% at 60 s and it became steady after 67.2 s for VLSFO. It is obvious that increasing the aeration flow rate would increase gas volume fraction for both types of oily wastewater, which is in line with the observations in Soderberg's study (2014). The slight difference in gas volume fractions of two types of oily wastewater was associated with their difference in viscosity (Table 3.2) and drag force. Xing et al. (2013) concluded that when the liquid viscosity was less than 0.01 Pa·s, the viscosity had a negligible effect on the bubble breakup rate and gas volume fraction which was confirmed by the results of the present study.

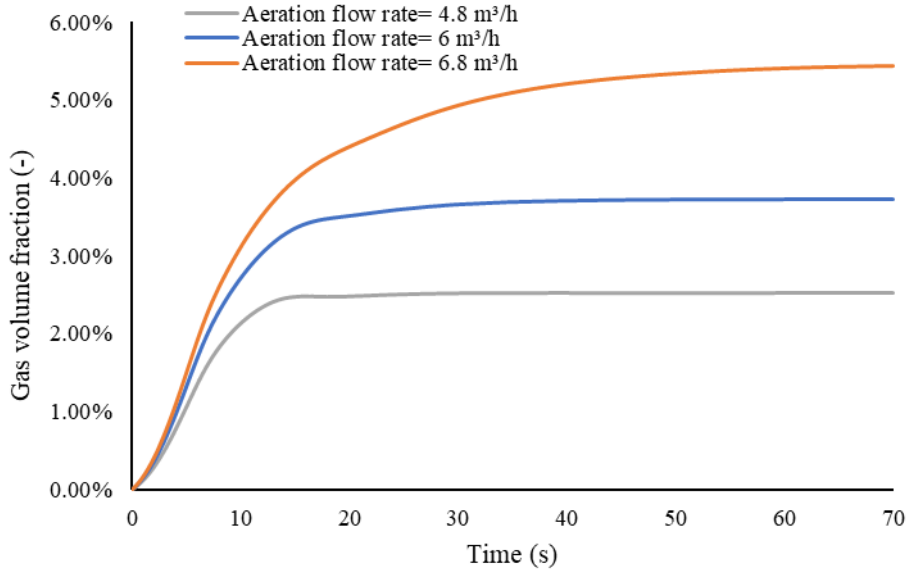

Figure 4.1 Gas volume fraction vs. time at different aeration flow rates in the system containing CLD wastewater

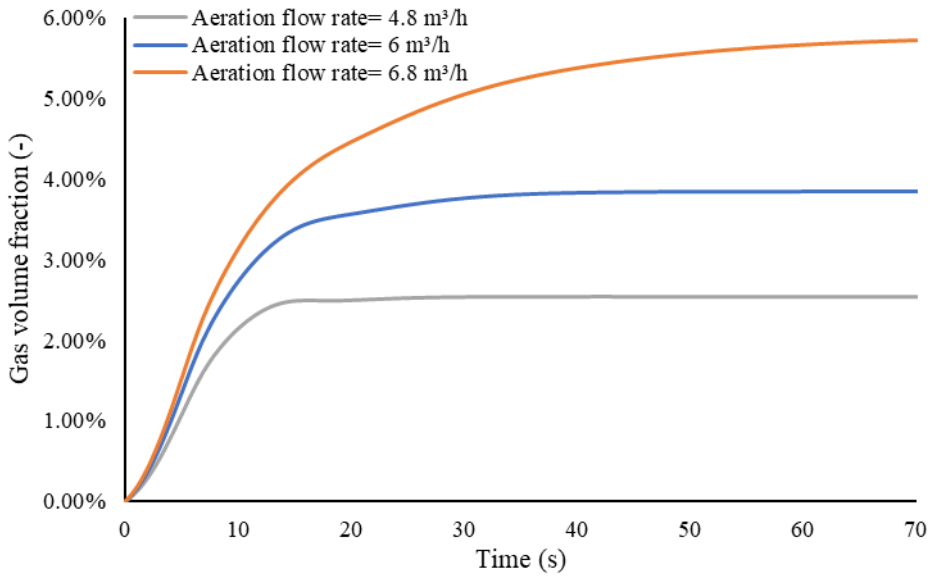

Figure 4.2 Gas volume fraction vs. time at different aeration flow rates in the system containing VLSFO wastewater

4.1.2. Impact of Aeration Flow Rate on Gas and Liquid Velocities in the Membrane Tank

Figure 4.3 (a-c) shows the liquid velocity arrow plots in the membrane tank at 70 s for three aeration flow rates (4.8, 6, and 6.8 m^3/h) under a permeate flow rate of 72 L/h when the system treats oily wastewater at a concentration of 100 mg/L of CLD. The color of arrow plots shows the quantity of gas velocity in different regions of the membrane tank where oily wastewater was circulating. Gas velocity near the walls of the membrane tank had the lowest amount (1 m/s). The reason would be attributed to the large size of the bubbles (average diameter: 4 mm); Jiang et al. (2016) showed that bubbles with large diameters preferred to move toward the middle part of the tank which was associated with the impact of lift force. The bottom side of the membrane tank close to air spargers had the

highest amount (i.e., between 3.5-5.5 m/s). Gas velocity close to the surface of the membrane tank was between 2-3 m/s where the gas exits the membrane tank.

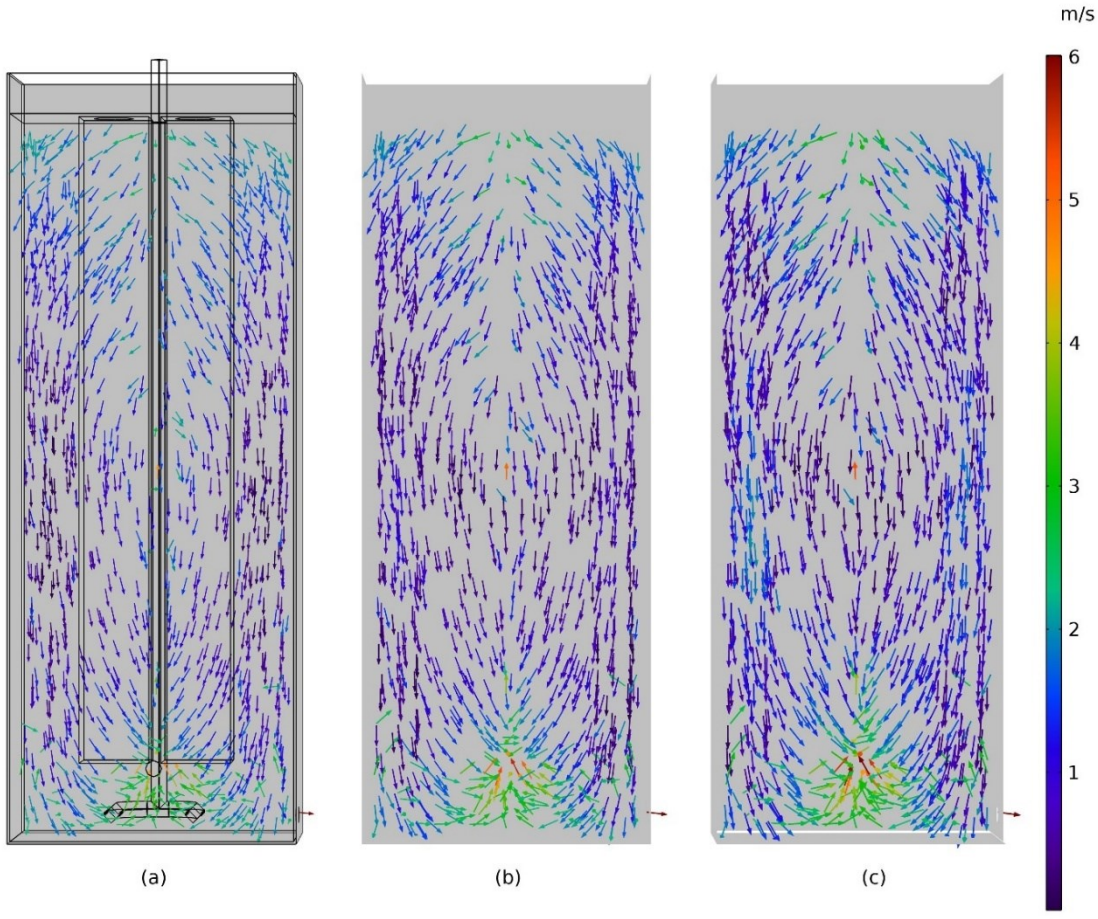

Figure 4.3 Liquid velocity arrow plots as a function of aeration rate at aeration flow rates of (a) 4.8, (b) 6, and (c) 6.8 m^3/h in the system containing CLD wastewater

As the aeration flow rate increased from 4.8 to 6.8 m^3/h, a circulating fluid flow with larger arrows was developed (as shown in Figure 4.3 (a-c)). In each figure, the whole fluid domain could be explained as a downward circulating flow region in the central domain above the aerator and the area close to the walls of the membrane tank. Previous studies obtained similar results and reported that as the gas flow rate increased, the system became

more unsteady (Akhondi et al., 2017; Bérubé, 2020) and most of the bubbles moved vigorously to the center of the tank. The down-flow of liquid close to the walls was proved by bubbles either flowing down or kept nearly stationary in that area (Torvik & Svendsen, 1990; Delnoij et al., 1997; Ndinisa et al., 2006). The same results were observed for the system containing VLSFO wastewater.

The changes in liquid velocities with time at various aeration flow rates were shown in Figure 4.4 and Figure 4.5 for two types of oily wastewater containing CLD and VLSFO, respectively. The volume average operator was used to measure liquid velocity in the membrane tank. When wastewater contained 100 mg/L of CLD at permeate flow rate of 72 L/h, liquid velocities reached 0.81, 1.06, and 1.81 m/s for the aeration flow rates of 4.8, 6, and 6.8 m^3/h, respectively (shown in Figure 4.4). When wastewater contained 100 mg/L of VLSFO at the same permeate flow rate, liquid velocities reached 0.83, 1.09, and 1.87 m/s for aeration flow rates of 4.8, 6, and 6.8 m^3/h, respectively (shown in Figure 4.5). Both figures showed that liquid velocity for two types of wastewater became stable at 15, 25, and 28 s when aeration flow rates were 4.8, 6, and 6.8 m^3/h, respectively. It was concluded that changing the type of oil did not have a significant influence on the liquid velocity condition and quantity since the difference in two types of wastewater viscosity and drag force were negligible. In addition, increasing the aeration flow rate led to an increase in the liquid velocity in two types of oil due to the agitation inside the tank generated by aerators; these results are similar to the observations of Brannock et al. (2010), Akhondi et al. (2017), and Du et al. (2017).

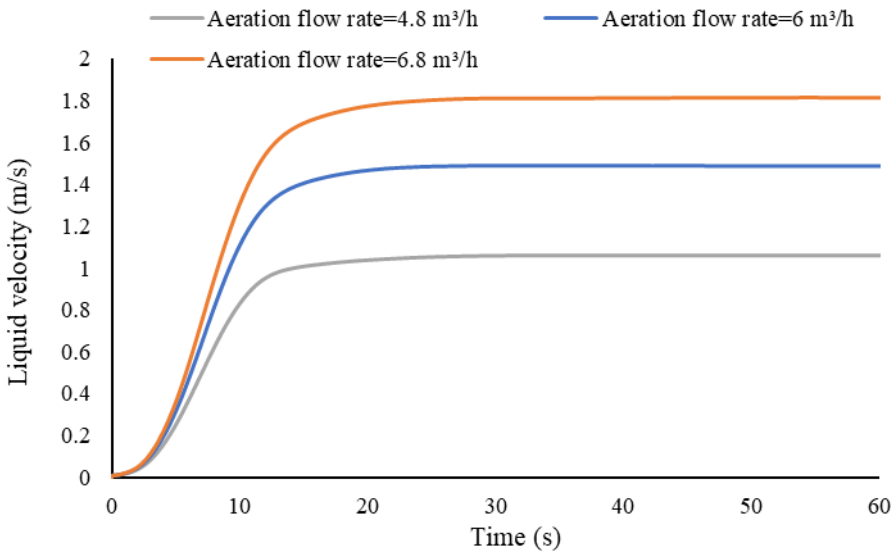

Figure 4.4 Liquid velocity vs. time at aeration flow rates of 4.8, 6, and 6.8 m^3/h in the system containing CLD wastewater

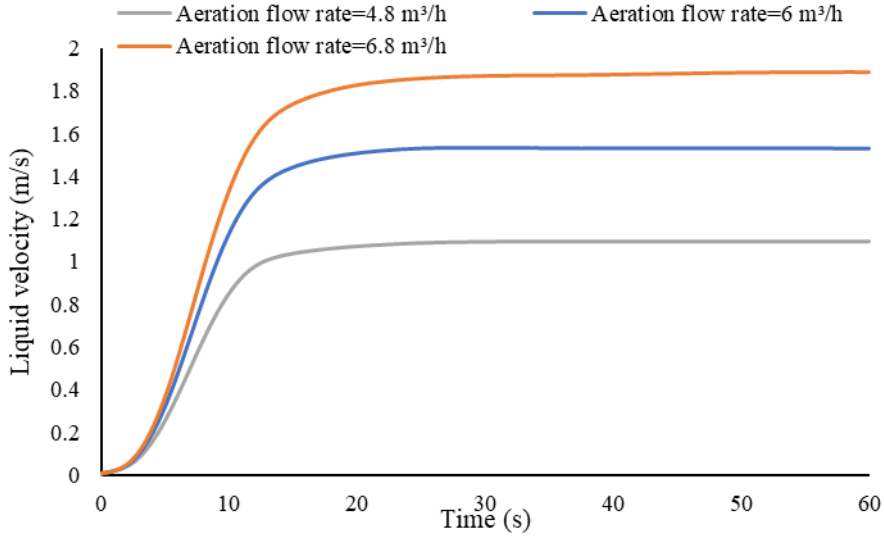

Figure 4.5 Liquid velocity vs. time at aeration flow rates of 4.8, 6, and 6.8 m^3/h in the system containing VLSFO wastewater

4.1.3. Impact of Aeration Flow Rate on Shear Rate and Shear Stress of the Membrane Surface

Figure 4.6 (a-c) shows the shear rate along the membrane treating CLD wastewater after reaching a stable condition. The surface average operator was applied for measuring the shear rate on the membrane surface. For an effective comparison of the plots, the maximum shear rate displayed in each plot has been fixed at 10 1/s. In this section, oil concentration (100 mg/L) and permeate flow rate (72 L/h) were constant and aeration flow rates were different. The shear rates ranged from 1 to 10 1/s and decreased between 4-8 1/s at a membrane module height of approximately 0.5 m in the middle of the membrane surface toward the top in Figure 4.6 (a-c). The top side of the membrane surface had a high shear rate (i.e., between 7-10 1/s), this was because of the quantity of gas velocity which was high in this area as shown in Figure 4.3 (a-c). The shear rate was higher when the aeration flow rate increased from 4.8 to 6.8 m^3/h (i.e., Figure 4.6a compared to Figure 4.6c) and there was the same condition for another type of oily wastewater.

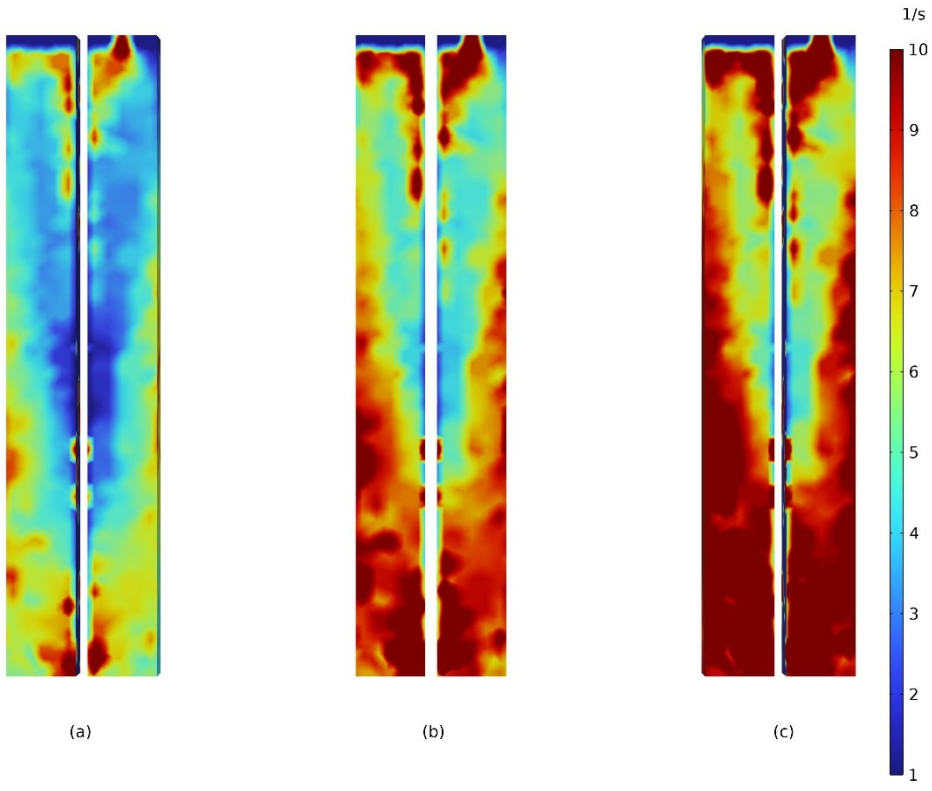

Figure 4.6 Shear rates along the membrane in a system containing CLD at three aeration flow rates of (a) 4.8, (b) 6, and (c) 6.8 m^3/h

In numerical modeling, the average shear rate and shear stress on the surface of the membranes at the aeration flow rates of 4.8, 6, and 6.8 m^3/h were obtained for the wastewater containing CLD and VLSFO as shown in Figure 4.7 and Figure 4.8. Fukano & Furukawa (1998) reported that liquid viscosity significantly affected the gas-liquid interfacial structure and interfacial shear stress. Therefore, the slight difference in shear stress was due to the fact that the dynamic viscosity of wastewater containing CLD was a little higher than the wastewater containing VLSFO. At the same quantity of aeration flow rate and the consequent shear rate, when the viscosity was a little higher in the wastewater

containing CLD, the shear stress was higher compared to VLSFO wastewater as shown in Figure 4.8.

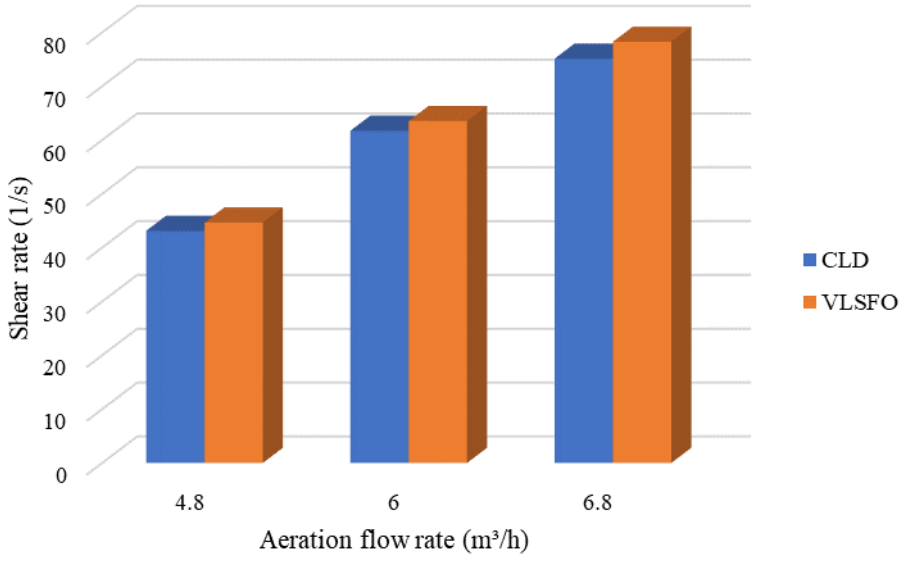

Figure 4.7 Shear rate along the membrane in a system containing CLD and VLSFO at three aeration flow rates

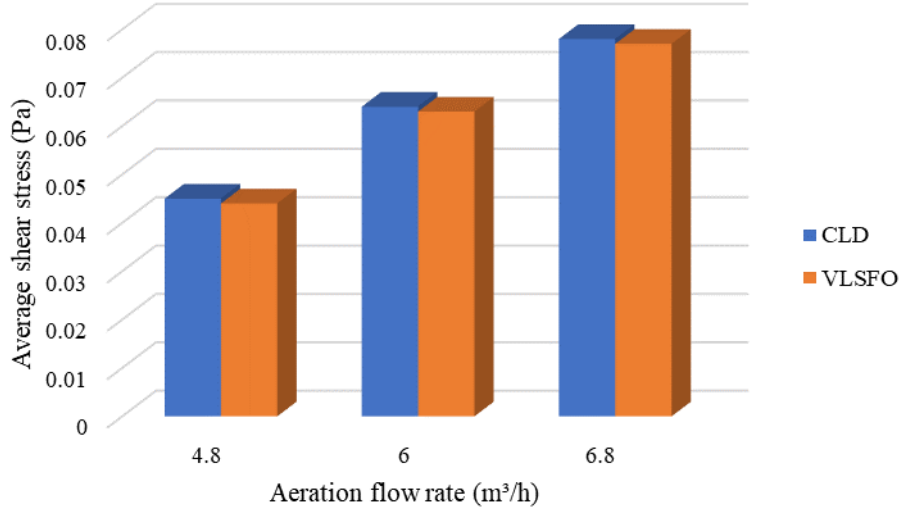

Figure 4.8 Shear stress along the membrane in a system containing CLD and VLSFO at three aeration flow rates

4.1.4. Impact of the Aeration on TMP

Using air sparging improves the membrane performance specifically in terms of decreasing membrane fouling (Bérubé, 2020). The vigorous movement of fluid in the membrane tank as a result of aeration increases turbulence and provides a homogenous condition for the fluid in the membrane tank (Braak et al., 2011; Khalili-Garakani et al., 2011). Aeration generates high shear forces that dislodges the foulants from the membrane surface in the membrane tank and mitigates membrane fouling (Wang et al., 2009; Bérubé, 2020). This was confirmed by numerical results; the effect of increasing aeration flow rate on average TMP under unsteady-state conditions was investigated and the time average quantity of TMP was shown in Figure 4.9 and Figure 4.10 for two types of wastewater containing CLD and VLSFO, respectively. The figures show the average TMP for aeration flow rates in the range of 4.8 to 6.8 m^3/h, the permeate flow rate of 72 L/h, and inlet oil concentrations in the range of 35 to 300 mg/L, for two types of oil. Figure 4.9 and Figure 4.10 show that TMP had mostly linear downward trends with increasing aeration flow rate in both types of oil similar to the results obtained by Wang et al. (2009) and Braak et al. (2011). This decrease was attributed to the cake layer thickness accumulated on the membrane surface that was removed gradually by an increase in aeration flow rate. The slope of TMP reduction vs. aeration flow rate in VLSFO was more than that of CLD (shown in Figure 4.10). This difference in both types of oil was associated with the physical properties of oil such as viscosity and molecular weight. They were less in light crude oil (i.e., VLSFO) and aeration flow rate could more easily sweep the light crude oil from the membrane surface and decreased the quantity of cake layer accumulated on the membrane surface.

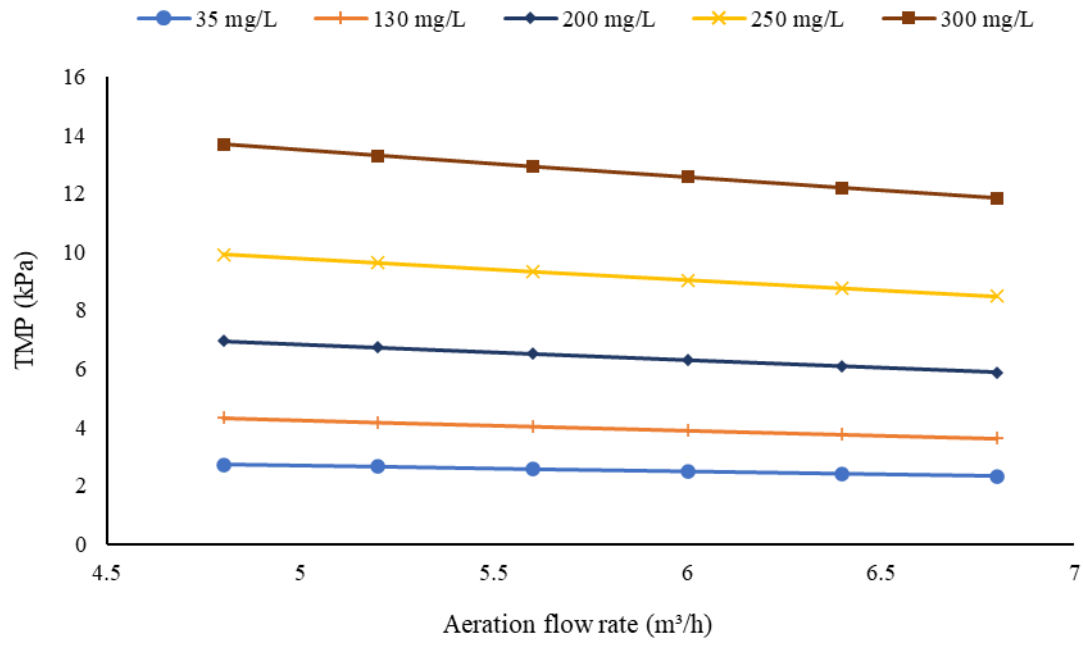

Figure 4.9 TMP vs. different aeration flow rates at various inlet concentrations of CLD

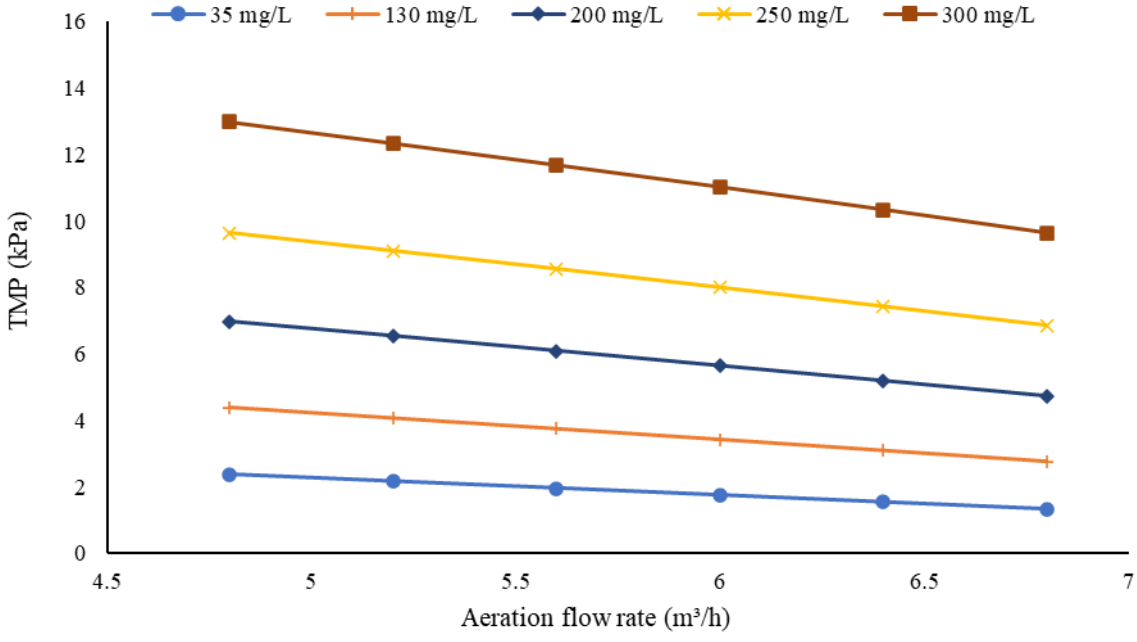

Figure 4.10 TMP vs. different aeration flow rates at various inlet concentrations of VLSFO

4.2. System Parametric Study

4.2.1. Impact of Inlet Oil Concentration on the System Performance

The effect of increasing inlet oil concentration on effluent oil concentration and average TMP under unsteady-state conditions for two types of wastewater containing CLD and VLSFO was analyzed and the time average quantity of each parameter was shown in Figure 4.11 and Figure 4.12. These figures show the predicted effluent oil concentration and average TMP for inlet oil concentrations in the range of 30 to 390 mg/L, the aeration flow rate of 4.8 m^3/h, and permeate flow rate of 72 L/h for two types of oily wastewater during 6 hours of operation. Based on the results in Figure 4.11, the effluent oil concentration in the CLD wastewater changed from 0.3132 to 42.24 mg/L for an inlet oil concentration in the range of 30 to 390 mg/L. Average TMP varied in the range of 2.69 to 20.26 kPa. Figure 4.12 shows the changes in the effluent oil concentration for VLSFO which were from 0.145 to 19.564 mg/L for an inlet oil concentration in the range of 30 to 390 mg/L and the average TMP increased from 2.29 to 19.6 kPa. Results showed that increasing inlet oil concentration to 270 mg/L met MARPOL 73/78 regulation when oily wastewater contained CLD, while in the VLSFO wastewater increasing oil concentration to 330 mg/L met MARPOL 73/78 regulation. By increasing inlet oil concentration from 30 to 390 mg/L, the oil removal efficiency was reduced from 98.96% to 89.17% for runs with CLD and in runs with VLSFO, it decreased from 99.5% to 94.98%. The possible reason was when the inlet oil concentration increased, the fouling formation on the surface of the membrane intensified, and as a result, the TMP increased. The more oil concentration was in the influent, the more oil concentration passed through the membrane

and when the concentration was high, the hydrophilic characteristics of the membrane could not impede the accumulation of oil on the membrane surface due to the decline in repulsion capability of the membrane, and consequently, the removal efficiency reduced (Kayvani Fard et al., 2018). These results are in line with Janknecht's et al. (2004) research who used polymeric UF and MF membranes to treat industrial cutting oil. They showed that increasing inlet oil concentration decreased the quality of permeate (Janknecht et al., 2004).

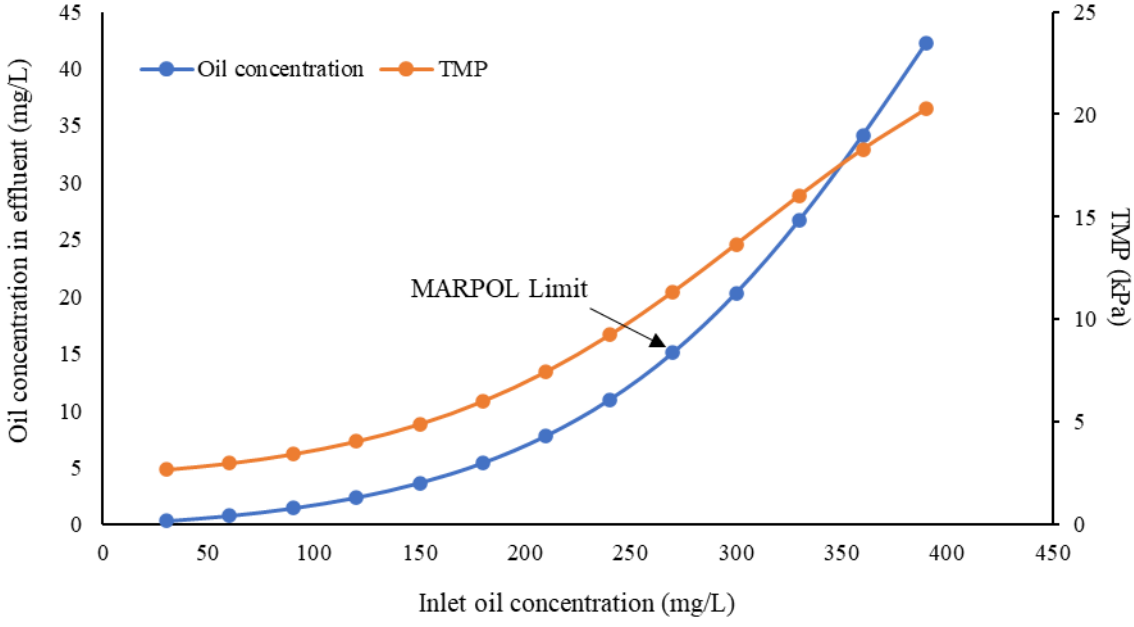

Figure 4.11 Effluent oil concentration and TMP vs. various inlet oil concentrations in the system containing CLD wastewater

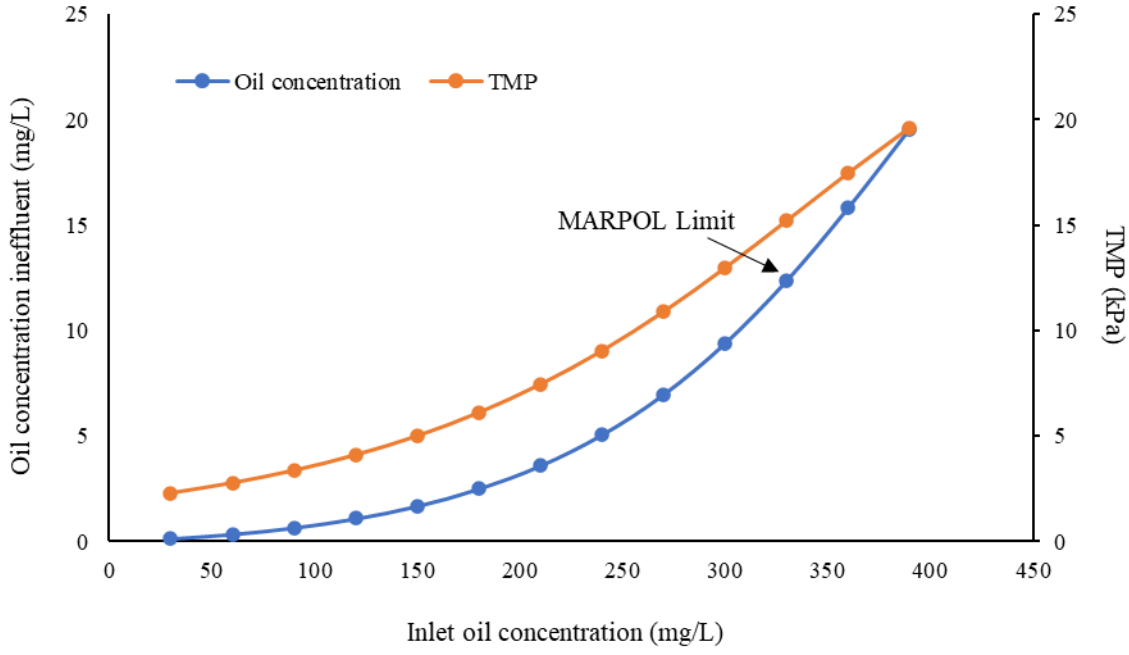

Figure 4.12 Effluent oil concentration and TMP vs. various inlet oil concentrations in the system containing VLSFO wastewater

4.2.2. Impact of Permeate Flow Rate on the System Performance

Figure 4.13 to Figure 4.16 show the effect of increasing permeate flow rate on effluent oil concentration and average TMP under unsteady-state conditions for two types of wastewater containing CLD and VLSFO. The figures show the effluent oil concentration and average TMP for permeate flow rates of 48, 72, 144, 216, 240 L/h, aeration flow rate of 4.8 m^3/h, and oil concentrations of 35, 50, 65, 80, 95, 110, 200, 300 mg/L for two types of oil. Based on the results, with an increase in the permeate flow rate the removal efficiency decreased and this reduction was more significant for higher oil concentrations such as 200 and 300 mg/L and at higher permeate flow rates as shown in Figure 4.13 and Figure 4.15. The decrease in the removal efficiency would be due to the higher convective

movement of oil particles through the membrane since high convective transport led to high surface tension forces between water and oil (Bird et al., 2002). Therefore, high oil movement across the membrane led to rapid transport of oil through the membrane. Tanudjaja et al. (2019) reported a lower permeate flow rate improved oil removal efficiency and permeate quality which was similar to the results of this study. Increasing inlet oil concentration caused more oil concentration to pass through the membrane. Oil removal efficiency significantly decreased due to the decrease in repulsion capability of the membrane as a result of the hydrophilic feature of the membrane that could not impede the oil accumulation on the membrane surface with the increase in oil concentration (Kayvani Fard et al., 2018). Comparing oily wastewater containing VLSFO with CLD wastewater, the concentration of effluent was lower than that of CLD as shown in Figure 4.13 and Figure 4.15. In addition, average TMP increased with increasing permeate flow rate in Figure 4.14 and Figure 4.16 similar to the results achieved by Germain et al. (2005). Because at higher permeate flow rates, pressure at two sides of the membrane increased based on Darcy's law. The changes of TMP were slightly lower in VLSFO than CLD due to the physical properties of the light oil as shown in Figure 4.16.

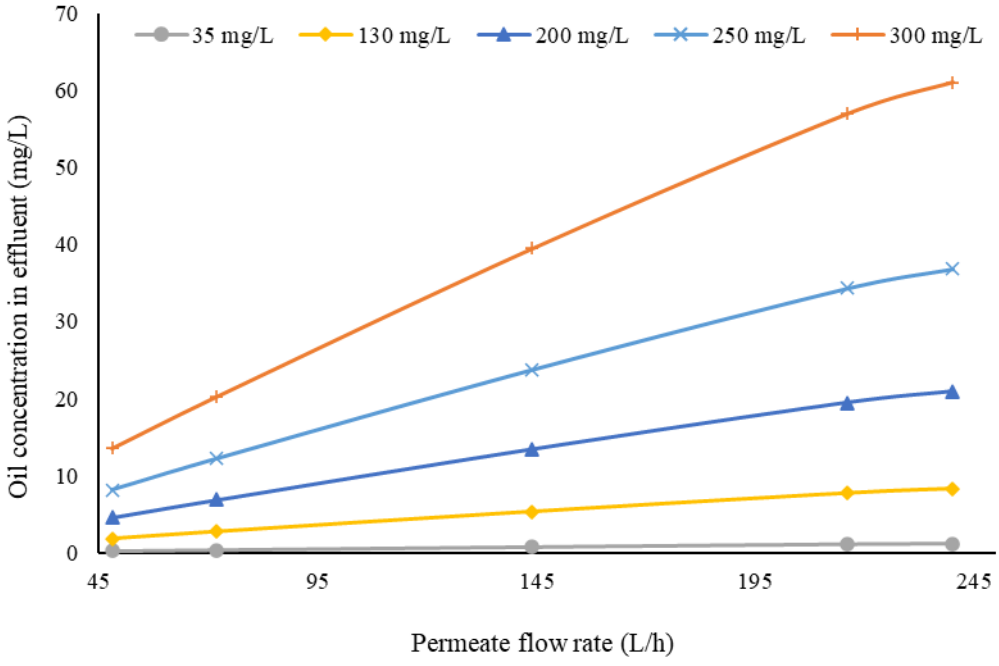

Figure 4.13 Effluent oil concentration vs. different permeate flow rates at various inlet concentrations of CLD

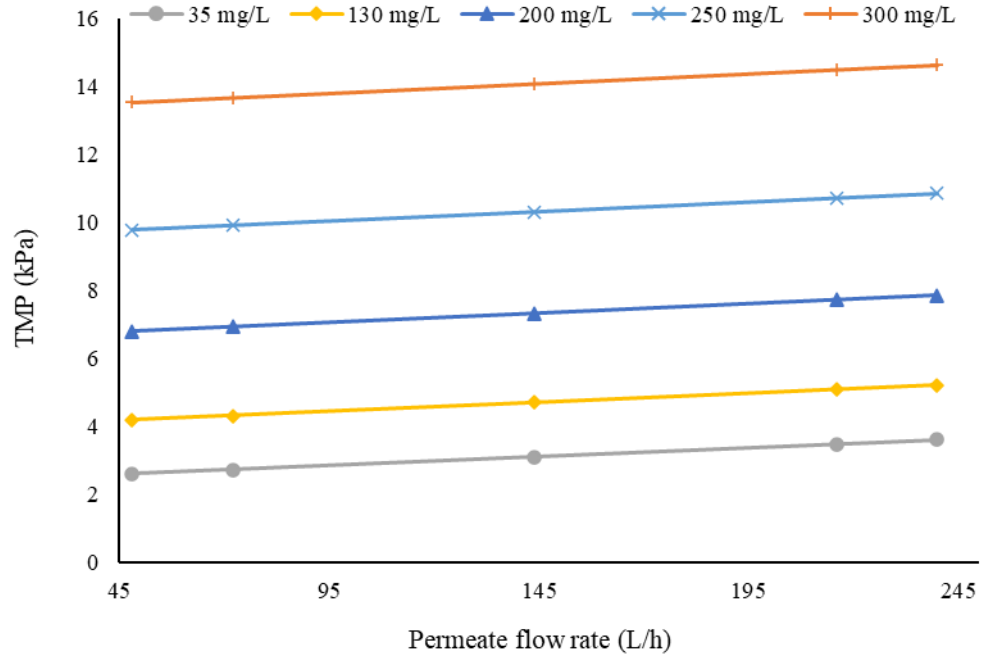

Figure 4.14 TMP vs. different permeate flow rates at various inlet concentrations of CLD

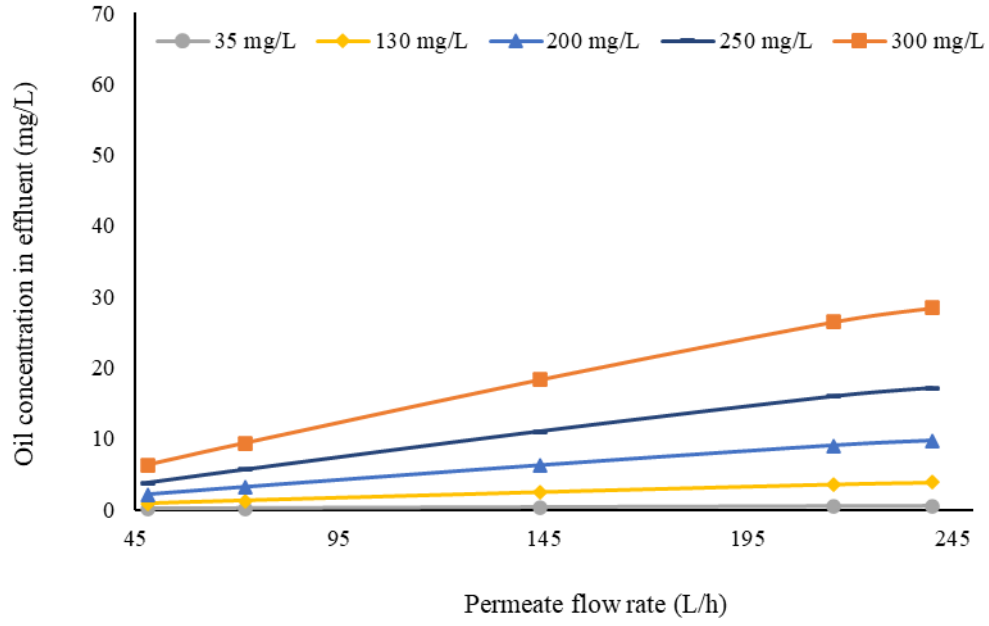

Figure 4.15 Effluent oil concentration vs. different permeate flow rates for various inlet concentrations of VLSFO

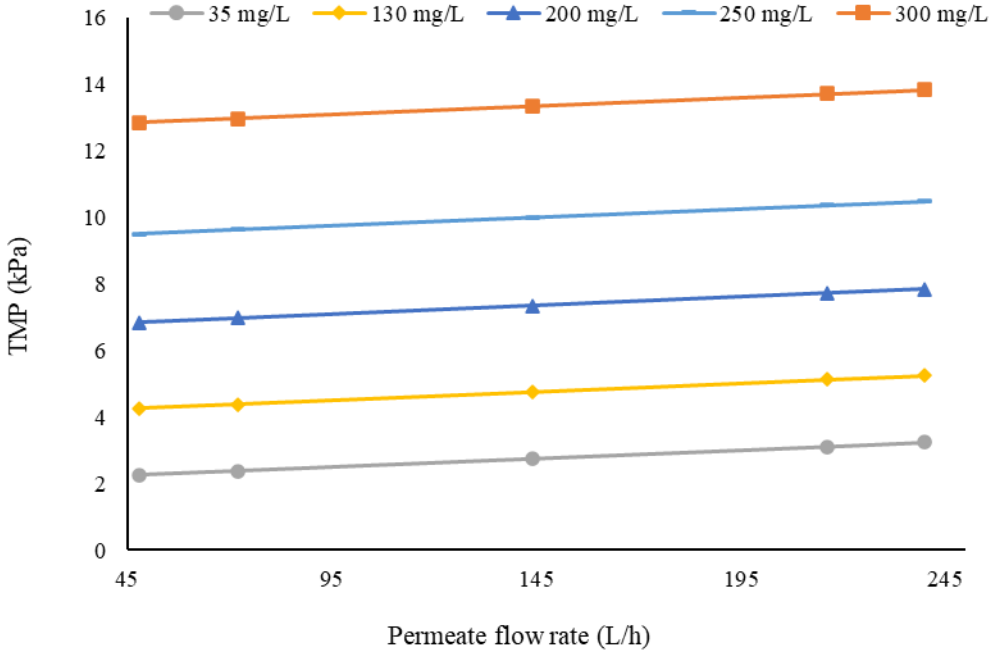

Figure 4.16 TMP vs. different permeate flow rates for various inlet concentrations of VLSFO

4.3. Investigation of TMP within 24-Hour Operations

This model was capable of predicting TMP for long-time operations; Figure 4.17 and Figure 4.18 show the changes of TMP in different inlet oil concentrations within 24 hours of filtration for two types of oily wastewater. TMP reached 38.91, 44.87, 50.12 kPa when the inlet oil concentrations for CLD were 45, 75, 95 mg/L, respectively which showed the need for chemical cleaning to restore the membrane permeability (Figure 4.17). This was due to the fact that at the constant membrane flux during long-term filtration process, the convection of foulants did not reduce and membrane fouling self-accelerated and led to a sharp increase of TMP (Le-Clech et al., 2006). Tummons et al. (2017) mentioned that at the beginning of the filtration, the deposited droplets partially blocked the pores of the membrane. When the filtration continued, more and more oil droplets were collected on the membrane surface and formed a cake layer. Since the droplets of oil were deformable, the consequent cake layer was firmly formed and created high resistance toward water permeation. TMPs were 34.098, 42.62, 49.40 kPa as shown in Figure 4.18, when the inlet oil concentrations for VLSFO were 45, 75, 95 mg/L, respectively. Lower increase in TMP for the system containing VLSFO would be related to the higher viscosity of CLD compared to VLSFO. The increase in TMP after 24 hours showed the requirement of chemical cleaning when TMP reached 40 kPa.

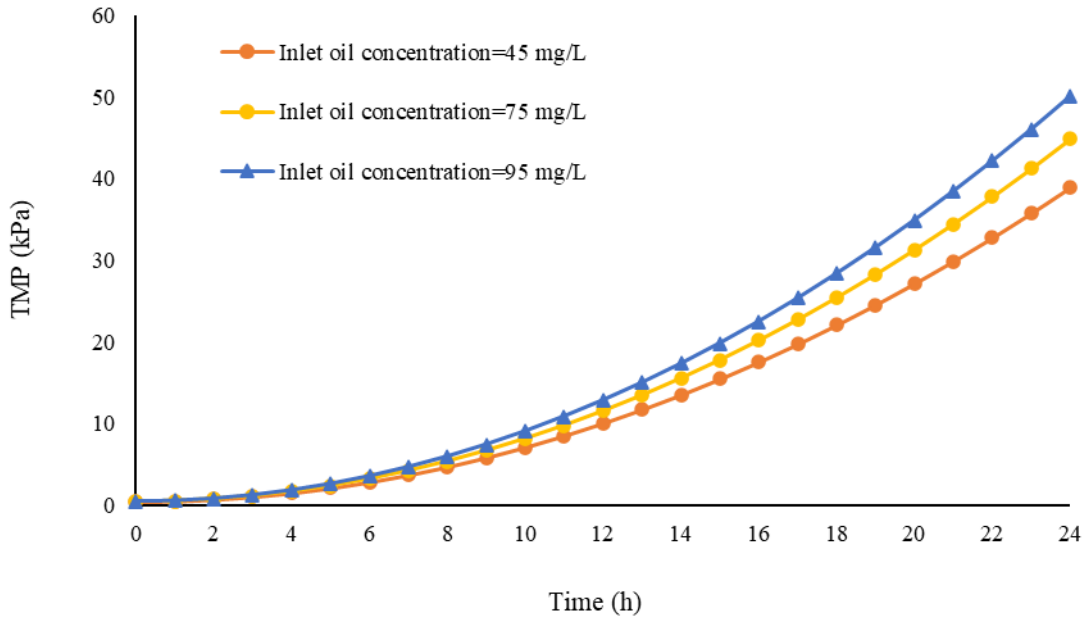

Figure 4.17 TMP vs. time for various inlet concentrations of CLD

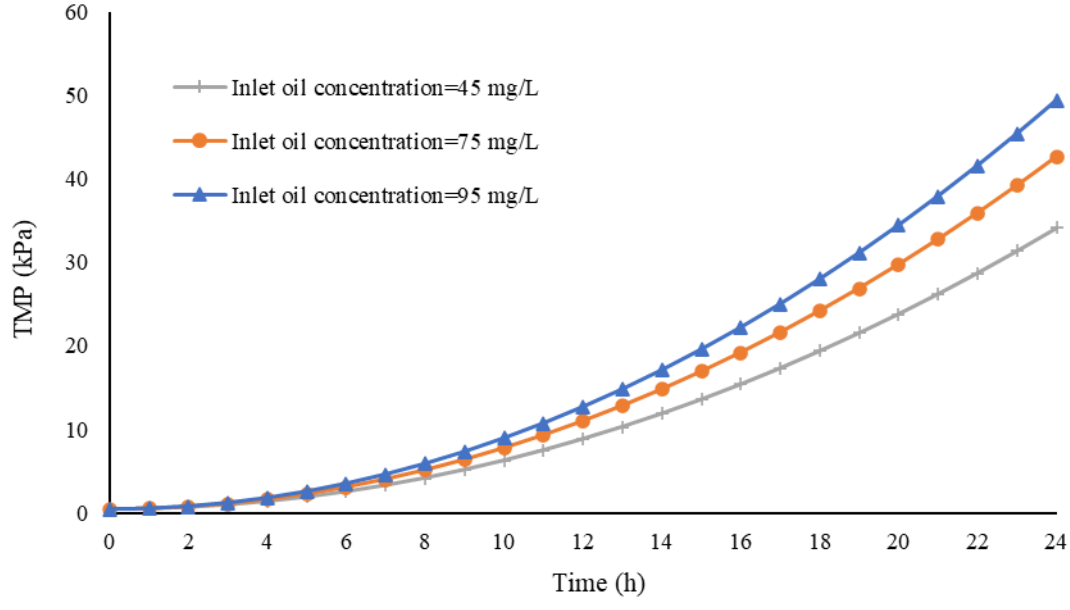

Figure 4.18 TMP vs. time for various inlet concentrations of VLSFO

4.4. Upscaling the System

Figure 4.19 shows the oil concentration in the effluent during the filtration time for different inlet oil concentrations of CLD and VLSFO. When oil concentration increased from 25 to 255 mg/L, the oil concentration in the effluent increased from 0.73 to 36.5 mg/L for CLD and from 0.34 to 17.15 mg/L for VLSFO as shown in Figure 4.19. The upscaled system met the MARPOL 73/78 regulation when the inlet oil concentration was up to 175 mg/L for CLD and 235 mg/L for VLSFO since the oil concentration in the effluent was 14.59 and 13.81 mg/L for CLD and VLSFO, respectively (shown in Figure 4.19). The oil removal efficiency in the upscaled system was achieved above 91% for different oil concentrations which showed the capability of the upscaled system to operate under 10,000 L/h and treated oily wastewater containing CLD and VLSFO during a 60-minute filtration. Figure 4.20 shows the average TMP changes in both types of oily wastewater with increasing oil concentration. It was observed that the average TMP had a slight difference in two types of oil, and it increased from 3.51 to 11.19 kPa for CLD and from 3.085 to 10.79 kPa for VLSFO as shown in Figure 4.20. This slight difference in average TMP changes would be due to a slight difference in the oily wastewater resistance against the flow which was attributed to viscosity.

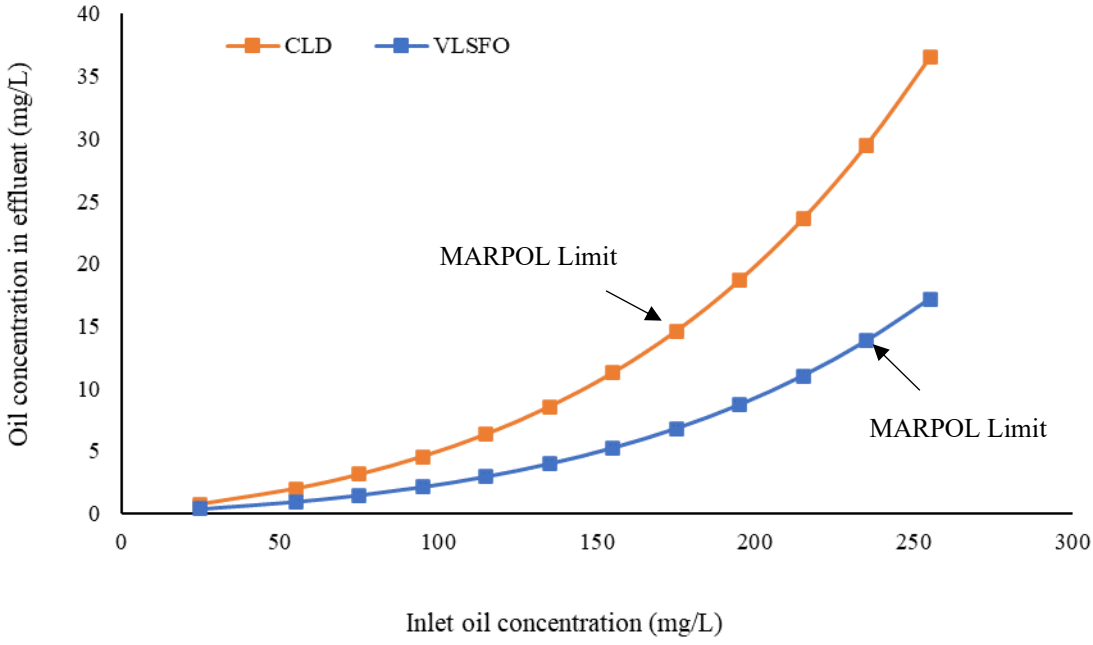

Figure 4.19 Effluent oil concentration vs. different inlet oil concentrations in oily wastewater containing CLD and VLSFO in the upscaled system

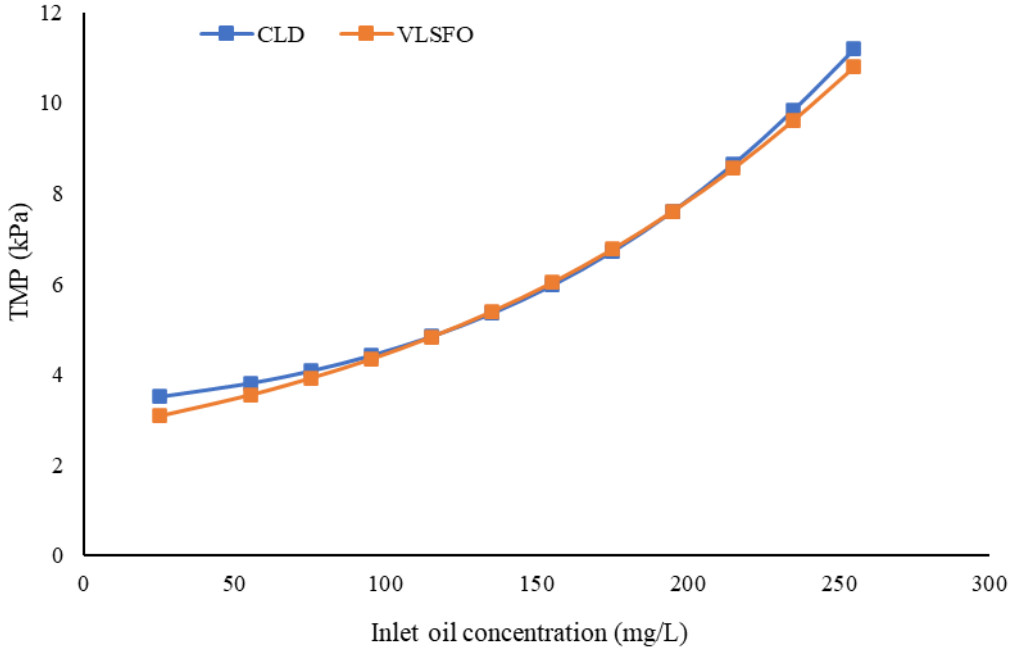

Figure 4.20 TMP vs. different inlet oil concentrations in oily wastewater containing CLD and VLSFO in the upscaled system

The effect of changing aeration flow rates on the average TMP for both light and heavy oil with inlet oil concentration of 95 mg/L was shown in Figure 4.21. This Figure shows that the decrease of TMP in VLSFO was more than that of CLD with increasing aeration flow rate. The low viscosity, density, and molecular weight of VLSFO caused foulants to be better removed from the membrane surface and TMP decreased more significantly which similarly obtained by Ghosh (2006).

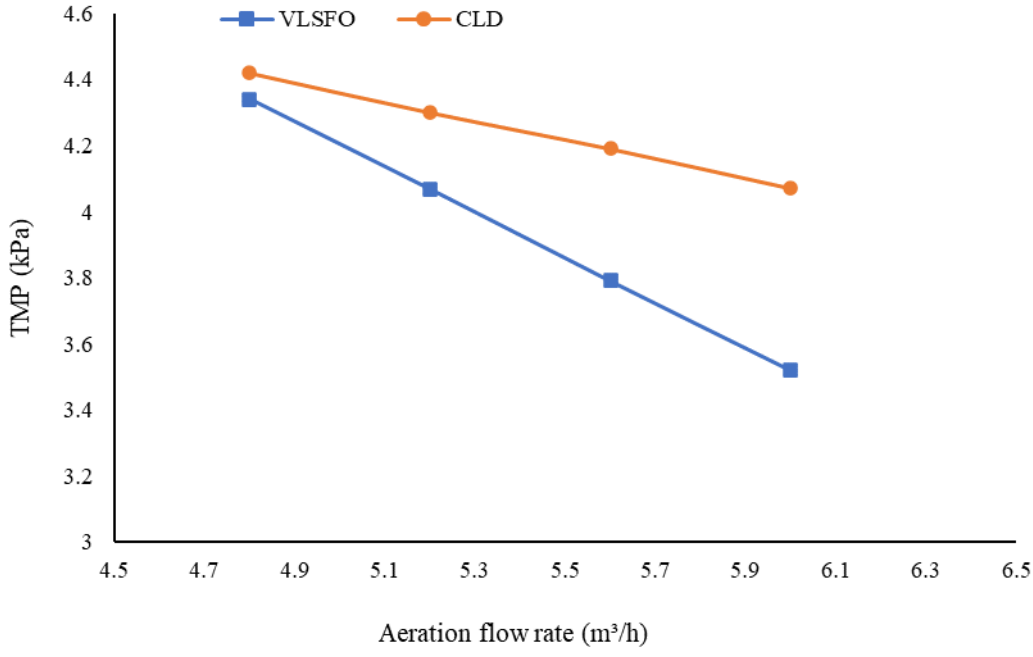

Figure 4.21 TMP vs. aeration flow rates for oily wastewater containing CLD and VLSFO in the upscaled system

In addition, the changes of TMP were investigated for both types of oily wastewater as shown in Figure 4.22 and Figure 4.23 for 24 hours. TMP rose to 39.79, 45.75, and 51 kPa for CLD in Figure 4.22 and 34.95, 43.48, 50.27 kPa for VLSFO in Figure 4.23. Yusuf et al. (2016) reported that in a long-term operation, total filtration performance was affected by the incremental filtration resistance as a result of the compact formation of fouling layer

on the surface of the membrane which led to a complete blockage of the membrane pores. The increase in TMP after 24 hours showed the requirement of chemical cleaning when TMP reached 40 kPa.

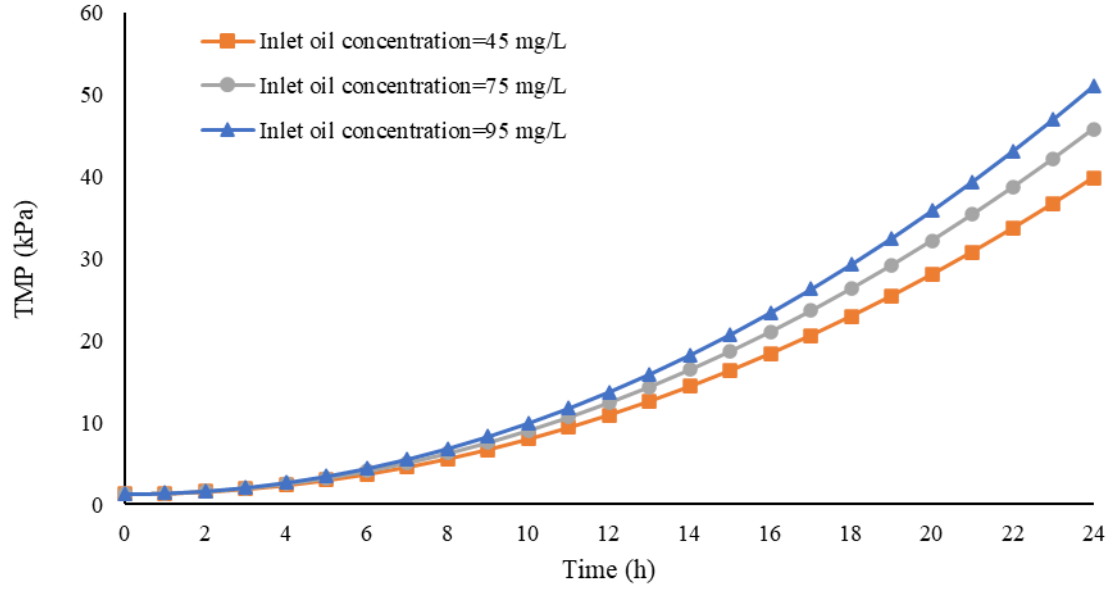

Figure 4.22 TMP vs. time for various inlet concentrations of CLD at permeate flow rate = 10,000 L/h during 24 hours

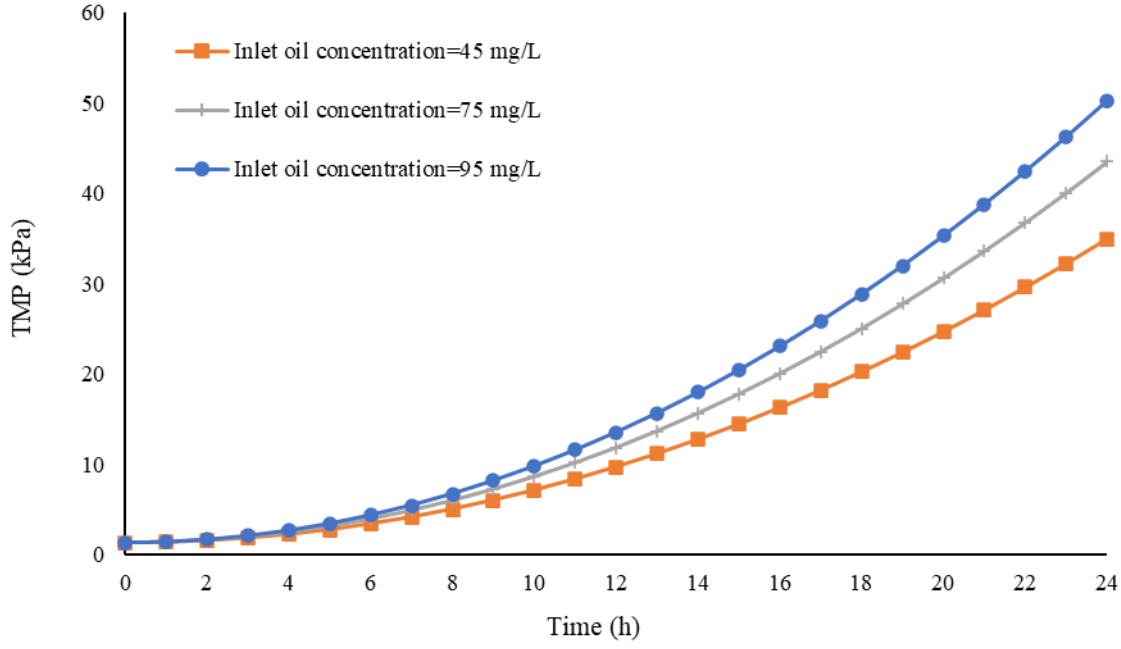

Figure 4.23 TMP vs. time for various inlet concentrations of VLSFO at permeate flow rate = 10,000 L/h during 24 hours

CHAPTER 5 CONCLUSION

5.1. Summary and Conclusion

This study simulated a pilot-scale membrane filtration system to treat oily wastewater under the constant flux using a 3D CFD model and investigate the effect of inlet oil concentration and permeate flow rate on oil removal efficiency and TMP during filtration process. In addition, the effect of aeration flow rate on TMP was assessed and the mechanism and hydrodynamic behaviour of the system were evaluated with two types of oily wastewater which has been challenging to determine in a real-world application. Upscaling investigation was also conducted to explore the capability and potential of the system as an onsite treatment technology for oil spill response operations through CFD modeling and this can save cost and energy for oil spill response team due to reducing the number of experimental runs.

The geometrical and operational parameters were used to design the 3D CFD model and governing equations related to fluid flow module, Darcy's law, and mass transport were determined and solved using the FEM in COMSOL Multiphysics. The model validation was fulfilled by oil removal efficiency and average TMP obtained by the experiments for each wastewater and the validated model was used for system parametric study and upscaling. To achieve the liquid and gas velocity distribution in the membrane tank, the fluid flow module was used. The first part of this study was conducted at an unsteady-state condition to investigate the hydrodynamics of the system. Following that, different CFD runs were conducted and showed that fluid flow in the membrane tank reached a steady state at a short simulation time. Therefore, this module was solved at a steady state in the

second part of the study to reduce computation time. The achieved velocity from the fluid flow module in the membrane tank was used in the mass transfer module. The velocity of the fluid in the membrane was estimated by Darcy's law in the membrane module and the achieved velocity was used in the porous media mass transfer module. After integrating three modules in three dimensions, the mass transfer module was solved in a time-dependent model to investigate the effluent oil concentration and TMP. This study was also conducted for 24-hour operations to predict TMP changes during the filtration time.

The obtained results from the proposed model were in a good agreement with the experimental results with a relative error of less than 5%. Results showed increasing inlet oil concentration to 270 mg/L met MARPOL 73/78 regulation when oily wastewater contained CLD, while in the wastewater containing VLSFO, increasing oil concentration to 330 mg/L met MARPOL 73/78 regulation. Increasing initial oil concentration increased TMP due to membrane fouling, and consequently, greater resistance occurred in the path of permeate transportation through the membrane. Aeration decreased TMP and reduced membrane fouling due to generating high shear force against the membrane and removing the foulants from the membrane surface. The developed model was further used to upscale a pilot-scale membrane filtration system for larger field-scale applications. The upscaled system was capable of treating 10,000 L/h of oily wastewater with the oil removal efficiency of more than 91%. Results demonstrated that the upscaled system met the MARPOL 73/78 regulation when the inlet oil concentration was up to 175 mg/L for CLD and 235 mg/L for VLSFO. In addition, the investigation of 24-hour filtrations showed the increase in TMP and the requirement of chemical cleaning to restore the membrane permeability during the filtration operation. The application of the upscaled system in oil

spill response will increase the capacity and improve the efficiency of oil spill response operations by increasing the space on storage barges and reducing the number of trips to shore.

5.2. Recommendations

The following recommendations will help to improve the investigation for future research.

- Since membrane fouling is a challenging issue in the membrane filtration technology treating oily wastewater, integrating backwashing and air scouring in the membrane cleaning process and modeling them is recommended. In addition, investigation and visualization of the fouling layers on the membrane surface in a pilot-scale membrane filtration system is suggested to understand what is happening on each layer of the membrane during the filtration process.
- Considering the impact of air bubble diameter changes with increasing aeration flow rate on membrane fouling and oil removal efficiency during filtration time in the pilot-scale membrane filtration system is recommended.
- Investigating the effect of feed outlet location on flow condition and hydrodynamic mechanism inside the membrane tank can be useful. It is recommended that feed outlet is placed on top of the membrane tank and the results compare with the previous achieved results.
- In a system equipped with HF membranes, each hollow fiber is vibrated as a result of aeration, and this can affect the performance of the membrane to treat oily wastewater. Therefore, considering the hollow fibers would be helpful to achieve a better understanding of a system performance and efficiency.

REFERENCES

Abdelrasoul, A., Doan, H., Lohi, A., & Cheng, C.-H. (2015). Morphology Control of Polysulfone Membranes in Filtration Processes: A Critical Review. *ChemBioEng Reviews*, *2*(1), 22–43. https://doi.org/10.1002/cben.201400030

Abuhasel, K., Kchaou, M., Alquraish, M., Munusamy, Y., & Jeng, Y. T. (2021). Oily wastewater treatment: Overview of conventional and modern methods, challenges, and future opportunities. *Water*, *13*(7), 7. https://doi.org/10.3390/w13070980

Ahmad, F., Lau, K. K., Shariff, A. M., & Murshid, G. (2012). Process simulation and optimal design of membrane separation system for CO2 capture from natural gas. *Computers & Chemical Engineering*, *36*, 119–128. https://doi.org/10.1016/j.compchemeng.2011.08.002

Akhondi, E., Zamani, F., Tng, K. H., Leslie, G., Krantz, W. B., Fane, A. G., & Chew, J. W. (2017). The performance and fouling control of submerged hollow fiber (HF) systems: A review. *Applied Sciences*, *7*(8), 8. https://doi.org/10.3390/app7080765

Al-Abbasi, O., & Shams, M. B. (2019). Transient CFD modelling of a full cycle dead-end ultrafiltration membrane. *2019 8th International Conference on Modeling Simulation and Applied Optimization (ICMSAO)*, 1–4. https://doi.org/10.1109/ICMSAO.2019.8880424

Al-Ghouti, M. A., Al-Kaabi, M. A., Ashfaq, M. Y., & Da'na, D. A. (2019). Produced water characteristics, treatment and reuse: A review. *Journal of Water Process Engineering*, *28*, 222–239. https://doi.org/10.1016/j.jwpe.2019.02.001

Amini, E., Mehrnia, M. R., Mousavi, S. M., & Mostoufi, N. (2013). Experimental study and computational fluid dynamics simulation of a full-scale membrane bioreactor for municipal wastewater treatment application. *Industrial & Engineering Chemistry Research*, *52*(29), 9930–9939. https://doi.org/10.1021/ie400632y

Anderson, J. D. (1995). *Computational fluid dynamics: The basics with applications*. McGraw-Hill.

Asadi Tashvigh, A., Fouladitajar, A., & Zokaee Ashtiani, F. (2015). Modeling concentration polarization in crossflow microfiltration of oil-in-water emulsion using shear-induced diffusion; CFD and experimental studies. *Desalination*, *357*, 225–232. https://doi.org/10.1016/j.desal.2014.12.001

Bagheri, M., & Mirbagheri, S. A. (2018). Critical review of fouling mitigation strategies in membrane bioreactors treating water and wastewater. *Bioresource Technology*, *258*, 318–334. https://doi.org/10.1016/j.biortech.2018.03.026

Baig, N., Salhi, B., Sajid, M., & Aljundi, I. H. (2022). Recent Progress in Microfiltration/Ultrafiltration Membranes for Separation of Oil and Water Emulsions. *The Chemical Record*, (n/a), e202100320. https://doi.org/10.1002/tcr.202100320

Becker, S., Sokolichin, A., & Eigenberger, G. (1994). Gas-liquid flow in bubble columns and loop reactors: Part II. Comparison of detailed experiments and flow simulations. *Chemical Engineering Science*, *49*(24, Part 2), 5747–5762. https://doi.org/10.1016/0009-2509(94)00290-8

Behroozi, A. H., & Ataabadi, M. R. (2021). Improvement in microfiltration process of oily wastewater: A comprehensive review over two decades. *Journal of Environmental Chemical Engineering*, *9*(1), 104981. https://doi.org/10.1016/j.jece.2020.104981

Behroozi, A. H., Kasiri, N., & Mohammadi, T. (2019). Multi-phenomenal macroscopic investigation of cross-flow membrane flux in microfiltration of oil-in-water emulsion, experimental & computational. *Journal of Water Process Engineering*, *32*, 100962. https://doi.org/10.1016/j.jwpe.2019.100962

Berk, Z. (2009). Chapter 10-Membrane processes. In Z. Berk (Ed.), *Food Process Engineering and Technology* (pp. 233–257). Academic Press. https://doi.org/10.1016/B978-0-12-373660-4.00010-7

Berman, A. S. (1953). Laminar Flow in Channels with Porous Walls. *Journal of Applied Physics*, *24*(9), 1232–1235. https://doi.org/10.1063/1.1721476

Bérubé, P. R. (2020). Chapter 11-Air sparging for fouling control. In H. Y. Ng, T. C. A. Ng, H. H. Ngo, G. Mannina, & A. Pandey (Eds.), *Current Developments in Biotechnology and Bioengineering* (pp. 225–243). Elsevier. https://doi.org/10.1016/B978-0-12-819809-4.00011-5

Bird, R. B., Stewart, W. E., & Lightfoot, E. N. (2002). *Transport phenomena* (2nd ed.). John Wiley & Sons Ltd., New York. https://www.wiley.com/en-us/Transport+Phenomena%2C+Revised+2nd+Edition-p-9780470115398, http://dx.doi.org/10.1115/1.1424298

Blazek, J. (2015). Computational fluid dynamics: Principles and applications (3rd ed), Elsevier

Braak, E., Alliet, M., Schetrite, S., & Albasi, C. (2011). Aeration and hydrodynamics in submerged membrane bioreactors. *Journal of Membrane Science*, *379*(1), 1–18. https://doi.org/10.1016/j.memsci.2011.06.004

Brannock, M., Wang, Y., & Leslie, G. (2010). Mixing characterisation of full-scale membrane bioreactors: CFD modelling with experimental validation. *Water Research*, *44*(10), 3181–3191. https://doi.org/10.1016/j.watres.2010.02.029

Bucs, S. S., Valladares Linares, R., Marston, J. O., Radu, A. I., Vrouwenvelder, J. S., & Picioreanu, C. (2015). Experimental and numerical characterization of the water flow in spacer-filled channels of spiral-wound membranes. *Water Research*, *87*, 299–310. https://doi.org/10.1016/j.watres.2015.09.036

Bucs, Sz. S., Valladares Linares, R., van Loosdrecht, M. C. M., Kruithof, J. C., & Vrouwenvelder, J. S. (2014). Impact of organic nutrient load on biomass accumulation, feed channel pressure drop increase and permeate flux decline in membrane systems. *Water Research*, *67*, 227–242. https://doi.org/10.1016/j.watres.2014.09.005

Cachaza, E. M., Díaz, M. E., Montes, F. J., & Galán, M. A. (2009). Simultaneous Computational Fluid Dynamics (CFD) Simulation of the Hydrodynamics and Mass Transfer in a Partially Aerated Bubble Column. *Industrial & Engineering Chemistry Research*, *48*(18), 8685–8696. https://doi.org/10.1021/ie900314s

Cai, J. J., Hawboldt, K., & Abdi, M. A. (2016). Analysis of the effect of module design on gas absorption in cross flow hollow membrane contactors via computational fluid dynamics (CFD) analysis. *Journal of Membrane Science*, *520*, 415–424. https://doi.org/10.1016/j.memsci.2016.07.054

Cao, W., & Mujtaba, I. M. (2015). Simulation of vacuum membrane distillation process for desalination with Aspen Plus. *Industrial & Engineering Chemistry Research*, *54*(2), 672–680. https://doi.org/10.1021/ie502874c

Cao, Y. (2016). Examinations of the shear stress on MBR-membrane plates by a single bubble using CFD [Master Thesis, Technische Universität]. https://tuprints.ulb.tu-darmstadt.de/5273/

Chakrabarty, B., Ghoshal, A. K., & Purkait, M. K. (2008). Ultrafiltration of stable oil-in-water emulsion by polysulfone membrane. *Journal of Membrane Science*, *325*(1), 427–437. https://doi.org/10.1016/j.memsci.2008.08.007

Completo, C., Semiao, V., & Geraldes, V. (2016). Efficient CFD-based method for designing cross-flow nanofiltration small devices. *Journal of Membrane Science*, *500*, 190–202. https://doi.org/10.1016/j.memsci.2015.11.012

COMSOL. (2022). Partition condition. https://doc.comsol.com/5.6/doc/com.comsol.help.chem/chem_ug_chemsptrans.08.064.html (Access on May 2021)

Cortés-Juan, F., Balannec, B., & Renouard, T. (2011). CFD-assisted design improvement of a bench-scale nanofiltration cell. *Separation and Purification Technology*, *82*, 177–184. https://doi.org/10.1016/j.seppur.2011.09.010

Damak, K., Ayadi, A., Zeghmati, B., & Schmitz, P. (2004). A new Navier-Stokes and Darcy's law combined model for fluid flow in crossflow filtration tubular membranes. *Desalination*, *161*(1), 67–77. https://doi.org/10.1016/S0011-9164(04)90041-0

Damak, K., Ayadi, A., Zeghmati, B., & Schmitz, P. (2005). Concentration polarisation in tubular membranes—A numerical approach. *Desalination*, *171*(2), 139–153. https://doi.org/10.1016/j.desal.2004.05.002

Darvishzadeh, T., & Priezjev, N. V. (2012). Effects of crossflow velocity and transmembrane pressure on microfiltration of oil-in-water emulsions. *Journal of Membrane Science*, *423–424*, 468–476. https://doi.org/10.1016/j.memsci.2012.08.043

De Morais Coutinho, C., Chiu, M. C., Basso, R. C., Ribeiro, A. P. B., Gonçalves, L. A. G., & Viotto, L. A. (2009). State of art of the application of membrane technology to vegetable oils: A review. *Food Research International*, *42*(5–6), 536–550. https://doi.org/10.1016/j.foodres.2009.02.010

Delnoij, E., Kuipers, J. A. M., & van Swaaij, W. P. M. (1997). Computational fluid dynamics applied to gas-liquid contactors. *Chemical Engineering Science*, *52*(21), 3623–3638. https://doi.org/10.1016/S0009-2509(97)00268-6

Deriszadeh, A., Husein, M. M., & Harding, T. G. (2010). Produced water treatment by micellar-enhanced ultrafiltration. *Environmental Science & Technology*, *44*(5), 1767–1772. https://doi.org/10.1021/es902862j

Dickhout, J. M., Moreno, J., Biesheuvel, P. M., Boels, L., Lammertink, R. G. H., & de Vos, W. M. (2017). Produced water treatment by membranes: A review from a colloidal perspective. *Journal of Colloid and Interface Science*, *487*, 523–534. https://doi.org/10.1016/j.jcis.2016.10.013

Dickinson, E. J. F., Ekström, H., & Fontes, E. (2014). COMSOL Multiphysics®: Finite element software for electrochemical analysis. A mini-review. *Electrochemistry Communications*, *40*, 71–74. https://doi.org/10.1016/j.elecom.2013.12.020

Du, X., Shi, Y., Jegatheesan, V., & Haq, I. U. (2020). A review on the mechanism, impacts and control methods of membrane fouling in MBR system. *Membranes*, *10*(2), 2. https://doi.org/10.3390/membranes10020024

Du, X., Wang, Y., Leslie, G., Li, G., & Liang, H. (2017). Shear stress in a pressure-driven membrane system and its impact on membrane fouling from a hydrodynamic condition perspective: A review. *Journal of Chemical Technology & Biotechnology*, *92*(3), 463–478. https://doi.org/10.1002/jctb.5154

Ebrahimi, M., Kerker, S., Daume, S., Geile, M., Ehlen, F., Unger, I., Schütz, S., & Czermak, P. (2015). Innovative ceramic hollow fiber membranes for recycling/reuse of oilfield produced water. *Desalination and Water Treatment*, *55*(13), 3554–3567. https://doi.org/10.1080/19443994.2014.947780

Emani, S., Uppaluri, R., & Purkait, M. K. (2014). Microfiltration of oil–water emulsions using low cost ceramic membranes prepared with the uniaxial dry compaction method. *Ceramics International*, *40*(1), 1155–1164. https://doi.org/10.1016/j.ceramint.2013.06.117

Fang, Q., Chen, J., Lu, C., Yin, D., & Li, Y. (2015). Study on relation between hydrodynamic feature size of HPAM and pore size of reservoir rock in Daqing oilfield. *Advances in Materials Science and Engineering*, *2015*.

Fasihi, M., Shirazian, S., Marjani, A., & Rezakazemi, M. (2012). Computational fluid dynamics simulation of transport phenomena in ceramic membranes for SO2 separation. *Mathematical and Computer Modelling*, *56*(11), 278–286. https://doi.org/10.1016/j.mcm.2012.01.010

Field, R. W., Wu, D., Howell, J. A., & Gupta, B. B. (1995). Critical flux concept for microfiltration fouling. *Journal of Membrane Science*, *100*(3), 259–272. https://doi.org/10.1016/0376-7388(94)00265-Z

Fimbres-Weihs, G. A., & Wiley, D. E. (2010). Review of 3D CFD modeling of flow and mass transfer in narrow spacer-filled channels in membrane modules. *Chemical Engineering and Processing: Process Intensification*, *49*(7), 759–781. https://doi.org/10.1016/j.cep.2010.01.007

Friedman, M., & Gillis, J. (1967). Viscous flow in a pipe with absorbing walls. *Journal of Applied Mechanics*, *34*(4), 819–822. https://doi.org/10.1115/1.3607840

Fukano, T., & Furukawa, T. (1998). Prediction of the effects of liquid viscosity on interfacial shear stress and frictional pressure drop in vertical upward gas–liquid annular flow. *International Journal of Multiphase Flow*, *24*(4), 587–603. https://doi.org/10.1016/S0301-9322(97)00070-0

Galvanin, F., Marchesini, R., Barolo, M., Bezzo, F., & Fidaleo, M. (2016). Optimal design of experiments for parameter identification in electrodialysis models. *Chemical Engineering Research and Design*, *105*, 107–119. https://doi.org/10.1016/j.cherd.2015.10.048

Germain, E., Stephenson, T., & Pearce, P. (2005). Biomass characteristics and membrane aeration: Toward a better understanding of membrane fouling in submerged membrane bioreactors (MBRs). *Biotechnology and Bioengineering*, *90*(3), 316–322. https://doi.org/10.1002/bit.20411

Ghidossi, R., Daurelle, J. V., Veyret, D., & Moulin, P. (2006a). Simplified CFD approach of a hollow fiber ultrafiltration system. *Chemical Engineering Journal*, *123*(3), 117–125. https://doi.org/10.1016/j.cej.2006.07.007

Ghidossi, R., Veyret, D., & Moulin, P. (2006b). Computational fluid dynamics applied to membranes: State of the art and opportunities. *Chemical Engineering and Processing: Process Intensification*, *45*(6), 437–454. https://doi.org/10.1016/j.cep.2005.11.002

Ghosh, R. (2006). Enhancement of membrane permeability by gas-sparging in submerged hollow fibre ultrafiltration of macromolecular solutions: Role of module design. *Journal of Membrane Science*, *274*(1–2), 73–82. https://doi.org/10.1016/j.memsci.2005.08.002

Gkotsis, P., Banti, D., Peleka, E., Zouboulis, A., & Samaras, P. (2014). Fouling issues in membrane bioreactors (MBRs) for wastewater treatment: Major mechanisms, prevention and control strategies. *Processes*, *2*(4), 795–866. https://doi.org/10.3390/pr2040795

Government of Canada. (2018). Canadian Environmental Protection Act. Available online: https://laws-lois.justice.gc.ca/eng/ acts/c-15.31/page-20.html#docCont (accessed on 20 July 2021).

Guo, X., Wang, Y., Zhang, H., Li, P., & Ma, C. (2017). Numerical and experimental investigation for cleaning process of submerged outside-in hollow fiber membrane. *Water Science and Technology*, *76*(6), 1283–1299. https://doi.org/10.2166/wst.2017.228

Habibi, S. (2014). An upscaled study of a membrane filtration process in presence of biofilms [Phd thesis, Ecole Centrale Paris]. https://tel.archives-ouvertes.fr/tel-01127571

Hamam, S. E. M., Hamoda, M. F., Shaban, H. I., & Kilani, A. S. (1988). Crude oil dissolution in saline water. *Water, Air, and Soil Pollution*, *37*(1), 55–64. https://doi.org/10.1007/BF00226479

Han, M., Zhang, J., Chu, W., Chen, J., & Zhou, G. (2019). Research progress and prospects of marine oily wastewater treatment: A review. *Water*, *11*(12), 12. https://doi.org/10.3390/w11122517

Hawkes, S., & M'Gonigle, M. (1992). A black (and rising) tide: Controlling maritime oil pollution in Canada. *Osgoode Hall Law Journal*, *30*(1), 165–260.

Hekmat, A., Amooghin, A. E., & Moraveji, M. K. (2010). CFD simulation of gas–liquid flow behaviour in an air-lift reactor: Determination of the optimum distance of the draft tube. *Simulation Modelling Practice and Theory*, *18*(7), 927–945. https://doi.org/10.1016/j.simpat.2010.02.009

Herndon, V. (2005). Transfer of decanting technology research to oil spill response organizations and regulators. https://www.bsee.gov/sites/bsee.gov/files/osrr-oil-spill-response-research/512aa.pdf (Access on June 2022)

Hesampour, M., Krzyzaniak, A., & Nyström, M. (2008). The influence of different factors on the stability and ultrafiltration of emulsified oil in water. *Journal of Membrane Science*, *325*(1), 199–208. https://doi.org/10.1016/j.memsci.2008.07.048

Hu, J., Ma, Y., Zhang, L., Gan, F., & Ho, Y.-S. (2010). A historical review and bibliometric analysis of research on lead in drinking water field from 1991 to 2007. *Science of The Total Environment*, *408*(7), 1738–1744. https://doi.org/10.1016/j.scitotenv.2009.12.038

Hussain, M. (2019). Modelling and prediction of non-linear scale-up from an Ultra Scale-Down membrane device to process scale tangential flow filtration [PhD thesis, University College London]. https://discovery.ucl.ac.uk/id/eprint/10078635/1/Hussain_10078635_thesis_sig-removed.pdf

Igunnu, E. T., & Chen, G. Z. (2014). Produced water treatment technologies. *International Journal of Low-Carbon Technologies*, *9*(3), 157–177. https://doi.org/10.1093/ijlct/cts049

ISCO. (2022). Guidelines for decanting settled out water. Available online:https://spillcontrol.org/2015/03/02/guidelines-for-decanting-settled-out-water (accessed on 9 April 2022)

Islam, M. R., & Hossain, M. E. (2021). Chapter 2-State-of-the-art of drilling. In M. R. Islam & M. E. Hossain (Eds.), *Drilling Engineering* (pp. 17–178). Gulf Professional Publishing. https://doi.org/10.1016/B978-0-12-820193-0.00002-2

Ismail, N. H., Salleh, W. N. W., Ismail, A. F., Hasbullah, H., Yusof, N., Aziz, F., & Jaafar, J. (2020). Hydrophilic polymer-based membrane for oily wastewater treatment: A review. *Separation and Purification Technology*, *233*, 116007. https://doi.org/10.1016/j.seppur.2019.116007

Izadi, A., Hosseini, M., Najafpour Darzi, G., Nabi Bidhendi, G., Pajoum Shariati, F., & Mosaddeghi, M. R. (2018). Perspectives on Membrane Bioreactor Potential for Treatment of Pulp and Paper Industry Wastewater: A Critical Review. *Journal of Applied Biotechnology Reports*, *5*(4), 139–150. https://doi.org/10.29252/JABR.05.04.02

Jalilvand, Z., Zokaee Ashtiani, F., Fouladitajar, A., & Rezaei, H. (2014). Computational fluid dynamics modeling and experimental study of continuous and pulsatile flow in flat sheet microfiltration membranes. *Journal of Membrane Science*, *450*, 207–214. https://doi.org/10.1016/j.memsci.2013.09.008

Janknecht, P., Lopes, A. D., & Mendes, A. M. (2004). Removal of industrial cutting oil from oil emulsions by polymeric ultra- and microfiltration membranes. *Environmental Science & Technology*, *38*(18), 4878–4883. https://doi.org/10.1021/es0348243

Jiang, X., Yang, N., & Yang, B. (2016). Computational fluid dynamics simulation of hydrodynamics in the riser of an external loop airlift reactor. *Particuology*, *27*, 95–101. https://doi.org/10.1016/j.partic.2015.05.011

Judd, S. (2010). The MBR book: Principles and applications of membrane bioreactors for water and wastewater treatment (2nd ed). Elsevier.

Judd, S. J. (2016). The status of industrial and municipal effluent treatment with membrane bioreactor technology. *Chemical Engineering Journal*, *305*, 37–45. https://doi.org/10.1016/j.cej.2015.08.141

Kallem, P., Othman, I., Ouda, M., Hasan, S. W., AlNashef, I., & Banat, F. (2021). Polyethersulfone hybrid ultrafiltration membranes fabricated with polydopamine modified ZnFe2O4 nanocomposites: Applications in humic acid removal and oil/water emulsion separation. *Process Safety and Environmental Protection*, *148*, 813–824. https://doi.org/10.1016/j.psep.2021.02.002

Kang, C.-W., Hua, J., Lou, J., Liu, W., & Jordan, E. (2008). Bridging the gap between membrane bio-reactor (MBR) pilot and plant studies. *Journal of Membrane Science*, *325*(2), 861–871. https://doi.org/10.1016/j.memsci.2008.09.016

Karpinska, A. M., & Bridgeman, J. (2018). CFD as a tool to optimize aeration tank design and operation. *Journal of Environmental Engineering* 144(2). http://hdl.handle.net/10454/15323

Kayvani Fard, A., Bukenhoudt, A., Jacobs, M., McKay, G., & Atieh, M. A. (2018). Novel hybrid ceramic/carbon membrane for oil removal. *Journal of Membrane Science*, *559*, 42–53. https://doi.org/10.1016/j.memsci.2018.05.003

Keir, G., & Jegatheesan, V. (2014). A review of computational fluid dynamics applications in pressure-driven membrane filtration. *Reviews in Environmental Science and Bio/Technology*, *13*(2), 183–201. https://doi.org/10.1007/s11157-013-9327-x

Keyvan Hosseini, P., Liu, L., Keyvan Hosseini, M., Bhattacharyya, A., Miao, J., & Wang, F. (2023). Treatment of a synthetic decanted oily seawater in a pilot-scale hollow fiber membrane filtration process: Experimental investigation. *Journal of Hazardous Materials*, *441*, 129928. https://doi.org/10.1016/j.jhazmat.2022.129928

Khalili-Garakani, A., Mehrnia, M. R., Mostoufi, N., & Sarrafzadeh, M. H. (2011). Analyze and control fouling in an airlift membrane bioreactor: CFD simulation and experimental studies. *Process Biochemistry*, *46*(5), 1138–1145. https://doi.org/10.1016/j.procbio.2011.01.036

Kim, D. C., & Chung, K. Y. (2019). Numerical simulation of aeration flow phenomena in bench-scale submerged flat membrane bioreactor. *Journal of Industrial and Engineering Chemistry*, *69*, 241–254. https://doi.org/10.1016/j.jiec.2018.09.014

Konstantinos Dionysios, P. (2015). *Modeling single & multi-phase flows in petroleum reservoirs using Comsol Multiphysics: "Pore to field-scale effects"* [Master Thesis, Technical University of Crete School of Mineral Resources Engineering]. https://dias.library.tuc.gr/view/33995

Koutsou, C. P., Yiantsios, S. G., & Karabelas, A. J. (2004). Numerical simulation of the flow in a plane-channel containing a periodic array of cylindrical turbulence promoters. *Journal of Membrane Science*, *231*(1), 81–90. https://doi.org/10.1016/j.memsci.2003.11.005

Kujawa, J., Cerneaux, S., Kujawski, W., & Knozowska, K. (2017). Hydrophobic ceramic membranes for water desalination. *Applied Sciences*, *7*(4), 4. https://doi.org/10.3390/app7040402

Kuzmin, D., & Turek, S. (2002). Flux correction tools for finite elements. *Journal of Computational Physics*, *175*(2), 525–558. https://doi.org/10.1006/jcph.2001.6955

Lalia, B. S., Kochkodan, V., Hashaikeh, R., & Hilal, N. (2013). A review on membrane fabrication: Structure, properties and performance relationship. *Desalination*, *326*, 77–95. https://doi.org/10.1016/j.desal.2013.06.016

Lateef, S. K., Soh, B. Z., & Kimura, K. (2013). Direct membrane filtration of municipal wastewater with chemically enhanced backwash for recovery of organic matter. *Bioresource Technology*, *150*, 149–155. https://doi.org/10.1016/j.biortech.2013.09.111

Le, N. L., & Nunes, S. P. (2016). Materials and membrane technologies for water and energy sustainability. *Sustainable Materials and Technologies*, *7*, 1–28. https://doi.org/10.1016/j.susmat.2016.02.001

Le-Clech, P., Chen, V., & Fane, T. A. G. (2006). Fouling in membrane bioreactors used in wastewater treatment. *Journal of Membrane Science*, *284*(1), 17–53. https://doi.org/10.1016/j.memsci.2006.08.019

Li, J., Jiang, C., Shi, W., Song, F., He, D., Miao, H., wang, T., Deng, J., & Ruan, W. (2018). Polytetrafluoroethylene (PTFE) hollow fiber AnMBR performance in the treatment of organic wastewater with varying salinity and membrane cleaning behavior. *Bioresource Technology*, *267*, 363–370. https://doi.org/10.1016/j.biortech.2018.07.063

Li, X., Li, J., Cui, Z., & Yao, Y. (2016). Modeling of filtration characteristics during submerged hollow fiber membrane microfiltration of yeast suspension under aeration condition. *Journal of Membrane Science*, *510*, 455–465. https://doi.org/10.1016/j.memsci.2016.03.003

Liu, B., Chen, B., Ling, J., Matchinski, E. J., Dong, G., Ye, X., Wu, F., Shen, W., Liu, L., Lee, K., Isaacman, L., Potter, S., Hynes, B., & Zhang, B. (2022). Development of advanced oil/water separation technologies to enhance the effectiveness of mechanical oil recovery operations at sea: Potential and challenges. *Journal of Hazardous Materials*, *437*, 129340. https://doi.org/10.1016/j.jhazmat.2022.129340

Liu, Y., He, G., Liu, X., Xiao, G., & Li, B. (2009). CFD simulations of turbulent flow in baffle-filled membrane tubes. *Separation and Purification Technology*, *67*(1), 14–20. https://doi.org/10.1016/j.seppur.2009.02.022

Lotfiyan, H., Zokaee Ashtiani, F., Fouladitajar, A., & Armand, S. B. (2014). Computational fluid dynamics modeling and experimental studies of oil-in-water emulsion microfiltration in a flat sheet membrane using Eulerian approach. *Journal of Membrane Science*, *472*, 1–9. https://doi.org/10.1016/j.memsci.2014.08.036

Lukitsch, B., Ecker, P., Elenkov, M., Janeczek, C., Haddadi, B., Jordan, C., Krenn, C., Ullrich, R., Gfoehler, M., & Harasek, M. (2020). Computation of global and local mass transfer in hollow fiber membrane modules. *Sustainability*, *12*(6), 6. https://doi.org/10.3390/su12062207

Maarefian, M., Miri, T., Sanaeepur, H., Rooeentan, H., & Azami, S. (2017). CFD simulation of a membrane bioreactor for high saline refinery wastewater treatment. *Desalination and Water Treatment*, *81*, 33–39. https://doi.org/10.5004/dwt.2017.21040

Madadi Avargani, V., & Divband, M. (2022). Performance evaluation of a solar water heating system with glass-covered parabolic trough concentrators, under different system tracking modes. *Journal of Thermal Analysis and Calorimetry*, *147*(7), 4873–4888. https://doi.org/10.1007/s10973-021-10845-9

Madaeni, S. S., Gheshlaghi, A., & Rekabdar, F. (2013). Membrane treatment of oily wastewater from refinery processes. *Asia-Pacific Journal of Chemical Engineering*, *8*(1), 45–53. https://doi.org/10.1002/apj.1619

Malaeb, L., & Ayoub, G. M. (2011). Reverse osmosis technology for water treatment: State of the art review. *Desalination*, *267*(1), 1–8. https://doi.org/10.1016/j.desal.2010.09.001

Marriott, J., & Sørensen, E. (2003). A general approach to modelling membrane modules. *Chemical Engineering Science*, *58*(22), 4975–4990. https://doi.org/10.1016/j.ces.2003.07.005

Medeiros, A. D. M. de, Silva Junior, C. J. G. da, Amorim, J. D. P. de, Durval, I. J. B., Costa, A. F. de S., & Sarubbo, L. A. (2022). Oily wastewater treatment: Methods, challenges, and trends. *Processes*, *10*(4), 4. https://doi.org/10.3390/pr10040743

Meena, R. A. A., Yukesh Kannah, R., Sindhu, J., Ragavi, J., Kumar, G., Gunasekaran, M., & Rajesh Banu, J. (2019). Trends and resource recovery in biological wastewater treatment system. *Bioresource Technology Reports*, *7*, 100235. https://doi.org/10.1016/j.biteb.2019.100235

Mueller, J., Cen, Y., & Davis, R. H. (1997). Crossflow microfiltration of oily water. *Journal of Membrane Science*, *129*(2), 221–235. https://doi.org/10.1016/S0376-7388(96)00344-4

Mukherjee, R., Bhunia, P., & De, S. (2016). Impact of graphene oxide on removal of heavy metals using mixed matrix membrane. *Chemical Engineering Journal*, *292*, 284–297. https://doi.org/10.1016/j.cej.2016.02.015

Mukherjee, R., Bhunia, P., & De, S. (2019). Long term filtration modelling and scaling up of mixed matrix ultrafiltration hollow fiber membrane: A case study of chromium(VI) removal. *Journal of Membrane Science*, *570–571*, 204–214. https://doi.org/10.1016/j.memsci.2018.10.026

Munirasu, S., Haija, M. A., & Banat, F. (2016). Use of membrane technology for oil field and refinery produced water treatment—A review. *Process Safety and Environmental Protection*, *100*, 183–202. https://doi.org/10.1016/j.psep.2016.01.010

Muradoglu, M., & Tasoglu, S. (2010). A front-tracking method for computational modeling of impact and spreading of viscous droplets on solid walls. *Computers & Fluids*, *39*(4), 615–625. https://doi.org/10.1016/j.compfluid.2009.10.009

Naim, R., Pei Sean, G., Nasir, Z., Mokhtar, N. M., & Safiah Muhammad, N. A. (2021). Recent Progress and Challenges in Hollow Fiber Membranes for Wastewater Treatment and Resource Recovery. *Membranes*, *11*(11), 11. https://doi.org/10.3390/membranes11110839

Nassehi, V. (1998). Modelling of combined Navier–Stokes and Darcy flows in crossflow membrane filtration. *Chemical Engineering Science*, *53*(6), 1253–1265. https://doi.org/10.1016/S0009-2509(97)00443-0

Ndinisa, N. V., Fane, A. G., Wiley, D. E., & Fletcher, D. F. (2006). Fouling control in a submerged flat sheet membrane system: Part II—two-phase flow characterization and CFD simulations. *Separation Science and Technology*, *41*(7), 1411–1445. https://doi.org/10.1080/01496390600633915

Nowee, S. M., Taherian, M., Salimi, M., & Mousavi, S. M. (2017). Modeling and simulation of phenol removal from wastewater using a membrane contactor as a bioreactor. *Applied Mathematical Modelling*, *42*, 300–314. https://doi.org/10.1016/j.apm.2016.10.027

Obotey Ezugbe, E., & Rathilal, S. (2020). Membrane technologies in wastewater treatment: A review. *Membranes*, *10*(5), 89. https://doi.org/10.3390/membranes10050089

Otitoju, T. A., Ahmad, A. L., & Ooi, B. S. (2016). Polyvinylidene fluoride (PVDF) membrane for oil rejection from oily wastewater: A performance review. *Journal of Water Process Engineering*, *14*, 41–59. https://doi.org/10.1016/j.jwpe.2016.10.011

Pabby, A. K., Rizvi, S. S. H., & Requena, A. M. S. (2015). Handbook of membrane separations: Chemical, pharmaceutical, food, and biotechnological applications, (2nd ed). CRC Press.

Parvareh, A., Rahimi, M., Madaeni, S. S., & Alsairafi, A. A. (2011). Experimental and CFD Study on the Role of Fluid Flow Pattern on Membrane Permeate Flux. *Chinese Journal of Chemical Engineering*, *19*(1), 18–25. https://doi.org/10.1016/S1004-9541(09)60171-3

Pawloski, J. (2016). Scalability and Design of a Submerged Membrane Bioreactor for Municipal Wastewater Treatment [Doctoral dissertation, University of Guelph]. https://atrium.lib.uoguelph.ca/xmlui/bitstream/handle/10214/10016/Pawloski_Jennifer_201609_PhD.pdf?sequence=1

Petersson, L. (2020). Modeling transport phenomena with COMSOL Multiphysics [Master Thesis, Lund University, Department of Chemical Engineering]. https://lup.lub.lu.se/luur/download?func=downloadFile&recordOId=9029654&fileOId=9029861

Poormohamadian, S. J., Koolivand, H., Koolivand-Salooki, M., & Esfandyari, M. (2022). Numerical modeling of wastewater treatment using hollow fiber membrane contactors based on the stiff spring method. *South African Journal of Chemical Engineering*, *40*, 21–31. https://doi.org/10.1016/j.sajce.2022.01.003

Pozrikidis, C. (2009). Fluid dynamics: theory, computation, and numerical simulation (2nd ed). Springer US. https://doi.org/10.1007/978-0-387-95871-2

Rashid, N., Pradhan, S., & Mackey, H. R. (2022). Chapter 15-Sustainability of wastewater treatment. In M. H. El-Naas & A. Banerjee (Eds.), *Petroleum Industry Wastewater* (pp. 223–248). Elsevier. https://doi.org/10.1016/B978-0-323-85884-7.00008-4

Rautenbach, R., Knauf, R., Struck, A., & Vier, J. (1996). Simulation and design of membrane plants with AspenPlus. *Chemical Engineering & Technology*, *19*(5), 391–397. https://doi.org/10.1002/ceat.270190502

Ren, J., Chowdhury, M. R., Xia, L., Ma, C., Bollas, G. M., & McCutcheon, J. R. (2020). A computational fluid dynamics model to predict performance of hollow fiber membrane modules in forward osmosis. *Journal of Membrane Science*, *603*, 117973. https://doi.org/10.1016/j.memsci.2020.117973

Rezakazemi, M., Khajeh, A., & Mesbah, M. (2018). Membrane filtration of wastewater from gas and oil production. *Environmental Chemistry Letters*, *16*(2), 367–388. https://doi.org/10.1007/s10311-017-0693-4

Saeed, A., Vuthaluru, R., & Vuthaluru, H. B. (2015). Investigations into the effects of mass transport and flow dynamics of spacer filled membrane modules using CFD. *Chemical Engineering Research and Design*, *93*, 79–99. https://doi.org/10.1016/j.cherd.2014.07.002

Saeed, A., Vuthaluru, R., Yang, Y., & Vuthaluru, H. B. (2012). Effect of feed spacer arrangement on flow dynamics through spacer filled membranes. *Desalination*, *285*, 163–169. https://doi.org/10.1016/j.desal.2011.09.050

Samstag, R. W., Ducoste, J. J., Griborio, A., Nopens, I., Batstone, D. J., Wicks, J. D., Saunders, S., Wicklein, E. A., Kenny, G., & Laurent, J. (2016). CFD for wastewater treatment: An overview. *Water Science and Technology*, *74*(3), 549–563. https://doi.org/10.2166/wst.2016.249

Sánchez-Vargas, J., & Valdés-Parada, F. J. (2021). Multiscale modeling of a membrane bioreactor for the treatment of oil and grease rendering wastewaters. *Revista Mexicana de Ingeniería Química*, *20*(2), 2. https://doi.org/10.24275/rmiq/Fen2368

Sanghamitra, P., Mazumder, D., & Mukherjee, S. (2021). Treatment of wastewater containing oil and grease by biological method- a review. *Journal of Environmental Science and Health, Part A*, *56*(4), 394–412. https://doi.org/10.1080/10934529.2021.1884468

Santos, J. L. C., Geraldes, V., Velizarov, S., & Crespo, J. G. (2007). Investigation of flow patterns and mass transfer in membrane module channels filled with flow-aligned spacers using computational fluid dynamics (CFD). *Journal of Membrane Science*, *305*(1), 103–117. https://doi.org/10.1016/j.memsci.2007.07.036

Shi, Y., Wang, Z., Du, X., Gong, B., Jegatheesan, V., & Haq, I. U. (2021). Recent advances in the prediction of fouling in membrane bioreactors. *Membranes*, *11*(6), 6. https://doi.org/10.3390/membranes11060381

Sidney, L., & Srinivasa, S. (1964). High flow porous membranes for separating water from saline solutions (United States Patent No. US3133132A). https://patents.google.com/patent/US3133132A/en

Smith, S., Taha, T., & Cui, Z. (2002). Enhancing hollow fibre ultrafiltration using slug-flow—A hydrodynamic study. *Desalination*, *146*(1), 69–74. https://doi.org/10.1016/S0011-9164(02)00491-5

Soderberg, A. C. (2014). Chapter 6-Fermentation Design. In H. C. Vogel & C. M. Todaro (Eds.), Fermentation and Biochemical Engineering Handbook (3rd ed) (pp. 85–108). William Andrew Publishing. https://doi.org/10.1016/B978-1-4557-2553-3.00006-4

Stephenson, T., Brindle, K., Judd, S., & Jefferson, B. (2000). Membrane bioreactors for wastewater treatment. IWA Publishing.

Sterlitech. (2022). Q & A: Cross Flow Velocity. ResearchGate. https://www.researchgate.net/institution/Sterlitech-Corporation/post/Q-A-Cross-Flow-Velocity-5bbe1aba84a7c19c5c009f1b (Access on June 2022)

Tanudjaja, H. J., Hejase, C. A., Tarabara, V. V., Fane, A. G., & Chew, J. W. (2019). Membrane-based separation for oily wastewater: A practical perspective. *Water Research*, *156*, 347–365. https://doi.org/10.1016/j.watres.2019.03.021

Tarabara, V. V., & Wiesner, M. R. (2003). Computational fluid dynamics modeling of the flow in a laboratory membrane filtration cell operated at low recoveries. *Chemical Engineering Science*, *58*(1), 239–246. https://doi.org/10.1016/S0009-2509(02)00436-0

The Pennsylvania State University. (2020). PNG 301, Introduction to petroleum and natural gas engineering. https://www.e-education.psu.edu/png301/node/839 (Access on March 2022)

Theodore, L., & Ricci, F. (2010a). Membrane separation processes. In *Mass transfer operations for the practicing engineer* (pp. 407–438). John Wiley & Sons, Ltd. https://doi.org/10.1002/9780470602591.ch15

Theodore, L., & Ricci, F. (2010b). Transport phenomena vs unit operations approach. In *Mass transfer operations for the practicing engineer* (pp. 7–10). John Wiley & Sons, Ltd. https://doi.org/10.1002/9780470602591.ch2

Torvik, R., & Svendsen, H. F. (1990). Modelling of slurry reactors. A fundamental approach. *Chemical Engineering Science*, *45*(8), 2325–2332. https://doi.org/10.1016/0009-2509(90)80112-R

Tummons, E. N., Chew, J. W., Fane, A. G., & Tarabara, V. V. (2017). Ultrafiltration of saline oil-in-water emulsions stabilized by an anionic surfactant: Effect of surfactant concentration and divalent counterions. *Journal of Membrane Science*, *537*, 384–395. https://doi.org/10.1016/j.memsci.2017.05.012

Ullah, A., Tanudjaja, H. J., Ouda, M., Hasan, S. W., & Chew, J. W. (2021). Membrane fouling mitigation techniques for oily wastewater: A short review. *Journal of Water Process Engineering*, *43*, 102293. https://doi.org/10.1016/j.jwpe.2021.102293

Varjani, S., Joshi, R., Srivastava, V. K., Ngo, H. H., & Guo, W. (2020). Treatment of wastewater from petroleum industry: Current practices and perspectives. *Environmental Science and Pollution Research*, *27*(22), 27172–27180. https://doi.org/10.1007/s11356-019-04725-x

Vera, E. A., & Ruiz, J. R. (2012). Comparison between turbulent and laminar bubbly-flow for modeling H2/H2O separation. *Proceeding of the 2012 COMSOL Conference, Milan*.

Vinther, F., Pinelo, M., Brøns, M., Jonsson, G., & Meyer, A. S. (2014). Mathematical modelling of dextran filtration through hollow fibre membranes. *Separation and Purification Technology*, *125*, 21–36. https://doi.org/10.1016/j.seppur.2014.01.034

Wah, T. (1964). Laminar Flow in a Uniformly Porous Channel. *Aeronautical Quarterly*, *15*(3), 299–310. https://doi.org/10.1017/S0001925900010908

Wang, B., Zhang, Y., Zhang, G., Zhang, K., & Field, R. W. (2021). Innovation and optimization of aeration in free bubbling flat sheet MBRs. *Journal of Membrane Science*, *635*, 119522. https://doi.org/10.1016/j.memsci.2021.119522

Wang, J., Gao, X., Ji, G., & Gu, X. (2019). CFD simulation of hollow fiber supported NaA zeolite membrane modules. *Separation and Purification Technology*, *213*, 1–10. https://doi.org/10.1016/j.seppur.2018.12.017

Wang, L., Wang, H., Li, B., Wang, Y., & Wang, S. (2014). Novel design of liquid distributors for VMD performance improvement based on cross-flow membrane module. *Desalination*, *336*, 80–86. https://doi.org/10.1016/j.desal.2014.01.004

Wang, Y., Brannock, M., Cox, S., & Leslie, G. (2010). CFD simulations of membrane filtration zone in a submerged hollow fibre membrane bioreactor using a porous media approach. *Journal of Membrane Science*, *363*(1), 57–66. https://doi.org/10.1016/j.memsci.2010.07.008

Wang, Y., Brannock, M., & Leslie, G. (2009). Membrane bioreactors: Overview of the effects of module geometry on mixing energy. *Asia-Pacific Journal of Chemical Engineering*, *4*(3), 322–333. https://doi.org/10.1002/apj.248

Wang, Y., Chen, X., Zhang, J., Yin, J., & Wang, H. (2009). Investigation of microfiltration for treatment of emulsified oily wastewater from the processing of petroleum products. *Desalination*, *249*(3), 1223–1227. https://doi.org/10.1016/j.desal.2009.06.033

Wardeh, S., & Morvan, H. P. (2008). CFD simulations of flow and concentration polarization in spacer-filled channels for application to water desalination. *Chemical Engineering Research and Design*, *86*(10), 1107–1116. https://doi.org/10.1016/j.cherd.2008.04.010

Wendt, J. F., Anderson, J. D., & Von Karman Institute for Fluid Dynamics (Eds.). (2008). Computational fluid dynamics: An introduction (3rd ed). Springer.

Wibisono, Y., Cornelissen, E. R., Kemperman, A. J. B., van der Meer, W. G. J., & Nijmeijer, K. (2014). Two-phase flow in membrane processes: A technology with a future. *Journal of Membrane Science*, *453*, 566–602. https://doi.org/10.1016/j.memsci.2013.10.072

Xing, C., Wang, T., & Wang, J. (2013). Experimental study and numerical simulation with a coupled CFD–PBM model of the effect of liquid viscosity in a bubble column. *Chemical Engineering Science*, *95*, 313–322. https://doi.org/10.1016/j.ces.2013.03.022

Yan, X., Wu, Q., Sun, J., Liang, P., Zhang, X., Xiao, K., & Huang, X. (2016). Hydrodynamic optimization of membrane bioreactor by horizontal geometry modification using computational fluid dynamics. *Bioresource Technology*, *200*, 328–334. https://doi.org/10.1016/j.biortech.2015.10.050

Yang, C. (2020). Petrochemical wastewater and its treatment [Master Thesis, Centria University of Applied Sciences]. https://www.theseus.fi/handle/10024/344161

Yeh, T. C. J., Wierenga, P., Khaleel, R., & Glass, R. J. (2005). Isotropy and anisotropy. In D. Hillel (Ed.), *Encyclopedia of Soils in the Environment* (pp. 285–291). Elsevier. https://doi.org/10.1016/B0-12-348530-4/00385-4

Yusuf, Z., Abdul Wahab, N., & Sahlan, S. (2016). Fouling control strategy for submerged membrane bioreactor filtration processes using aeration airflow, backwash, and relaxation: A review. *Desalination and Water Treatment*, *57*(38), 17683–17695. https://doi.org/10.1080/19443994.2015.1086893

Zare, M., Zokaee Ashtiani, F., & Fouladitajar, A. (2013). CFD modeling and simulation of concentration polarization in microfiltration of oil–water emulsions; Application of an Eulerian multiphase model. *Desalination*, *324*, 37–47. https://doi.org/10.1016/j.desal.2013.05.022

Zhang, B., Huang, D., Shen, Y., Yin, W., Gao, X., Zhang, B., & Shi, W. (2020). Treatment of alkali/surfactant/polymer flooding oilfield wastewater with polytetrafluoroethylene microfiltration membrane: Performance and membrane fouling. *Journal of Environmental Chemical Engineering*, *8*(5), 104462. https://doi.org/10.1016/j.jece.2020.104462

Zhang, D., Dechatiwongse, P., & Hellgardt, K. (2015). Modelling light transmission, cyanobacterial growth kinetics and fluid dynamics in a laboratory scale multiphase photo-bioreactor for biological hydrogen production. *Algal Research*, *8*, 99–107. https://doi.org/10.1016/j.algal.2015.01.006

Zheng, G., & Price, W. S. (2012). Direct hydrodynamic radius measurement on dissolved organic matter in natural waters using diffusion NMR. *Environmental Science & Technology*, *46*(3), 1675–1680.

Zheng, J., Liu, B., Ping, J., Chen, B., Wu, H., & Zhang, B. (2015). Vortex- and shaker-assisted liquid–liquid microextraction (VSA-LLME) coupled with gas chromatography and mass spectrometry (GC-MS) for analysis of 16 polycyclic aromatic hydrocarbons (PAHs) in offshore produced water. *Water, Air, & Soil Pollution*, *226*(9), 318. https://doi.org/10.1007/s11270-015-2575-3

Zoubeik, M. F. (2018). Membrane Filtration System for Produced Water Treatment: Experimental and Modeling Analyses [Thesis, Faculty of Graduate Studies and Research, University of Regina]. https://ourspace.uregina.ca/handle/10294/8508